

MARINE RED STAINING OF A PENNSYLVANIAN CARBONATE SLOPE: ENVIRONMENTAL AND OCEANOGRAPHIC SIGNIFICANCE

BRAM VAN DER KOOIJ,¹ ADRIAN IMMENHAUSER,^{1,2} THOMAS STEUBER,³ MISCHA HAGMAIER,² JUAN R. BAHAMONDE,⁴
ELIAS SAMANKASSOU,⁵ AND OSCAR MERINO TOMÉ⁶

¹Faculty of Earth and Life Sciences, Vrije Universiteit Amsterdam, De Boelelaan 1085, 1081 HV Amsterdam, The Netherlands

²Ruhr Universität Bochum, Institut für Geologie, Mineralogie und Geophysik, Universitätsstrasse 150, 44801, Bochum, Germany

³Petroleum Institute, P.O. Box 2533, Abu Dhabi, United Arab Emirates

⁴Departamento de Geología, Area de Estratigrafía, Jesús Arias de Velasco s/n, 33005 Oviedo, Spain

⁵Institute of Geology and Paleontology, University of Fribourg, Pérolles, CH-1700 Fribourg, Switzerland

⁶School of Earth, Ocean and Planetary Sciences, Cardiff University, Main building, Park Place, Cardiff CF10 3YE, U.K.

e-mail: bram.van.der.kooij@falw.vu.nl

ABSTRACT: Red-stained platform facies are a common feature of many carbonate settings throughout the geological record. Although the mechanisms involved in red staining of subaerially exposed or argillaceous, peri-platform limestones are reasonably well understood, the environmental and oceanographic significance of red carbonates often remains uncertain. Here, sedimentological, sequence stratigraphic, geochemical, paleontological, and quantitative bathymetric data from Pennsylvanian red intervals across a well exposed carbonate platform top and slope are documented and interpreted in a process-oriented context. On the upper slope (80–350 meters below the shelf break), red intervals alternate with gray, mainly microbial algal boundstones. On the lower slope (350–600 meters below the shelf break), redeposited red-stained mud builds matrix-supported breccia tongues interbedded with predominantly redeposited, clast-supported carbonate debris. The presence of large volumes of fibrous calcite biocementstones as well as firmgrounds point to low sedimentation rates or omission. In terms of sequence stratigraphy, red intervals occur within maximum flooding intervals and reflect near platform drowning. Elevated $\delta^{18}\text{O}$ values (2–3‰) and an essentially cool-water, heterotrophic biotic association in red intervals on platform top and slope suggest deposition during sea-level highs, associated with colder water masses and high nutrient levels. The most likely drivers are an elevated thermocline and upwelling. The red staining is the result of iron oxidation which occurred during early diagenesis, likely by iron bacteria. These red intervals provide an important bathymetric benchmark against which other (mainly Paleozoic) red facies can be tested and calibrated.

INTRODUCTION

A wide spectrum of conspicuously red-stained platform to hemipelagic carbonate rocks is known from many marine and epeiric basins worldwide throughout the geological record (Fig. 1; Table 1). The deepest marine, (hemi) pelagic, *in situ* red carbonates known are Cretaceous oceanic red beds (CORB; Fig. 1; Hu et al. 2005, and references therein). CORBs are deposited at water depths near the calcite compensation depth (CCD). Perhaps the best-known red carbonate facies are the Jurassic "Condensed facies," the related "Ammonitico Rosso" (Jenkyns 1974), and the Devonian "Schwellenkalk" (Fig. 1; Tucker 1974; Jenkyns 1986). Whereas (hemi) pelagic "Condensed facies," "Schwellenkalk," and "Griotte" are deposited on submarine topographic highs, the (hemi) pelagic "Ammonitico Rosso," "Becken facies," "Knollenkalk" are restricted to topographic lows.

On ramps, red carbonates are described predominantly from the more distal portion (Fig. 1) such as in the Devonian Montagne Noire (southern France; Tucker 1974; Preat et al. 1999), the Jurassic Oolithe Ferrugineuse de Bayeux (northern France; Preat et al. 2000) and the Czorsztyn Unit (Slovakia; Jurassic; Aubrecht et al. 2002). Red carbonates in proximal ramp environments include the Krupianka Formation (Slovakia;

Jurassic; Aubrecht et al. 2002; Aubrecht and Szulc 2006) and the Devonian griotte of the Montagne Noire (Southern France; Preat et al. 1999).

Red carbonate mounds or buildups are known from shallow-water environments within the photic zone, platform top, inner and outer ramp setting, from submarine highs and from deeper-water environments (Fig. 1). Examples of red carbonate mounds and buildups include the Cambrian red bioherms of the Flinders Range (James and Gravestock 1990), the Devonian Récifs Rouges (Belgium; Bourque and Boulvain 1993; Boulvain 2001; Boulvain et al. 2001), Carboniferous mounds in the Picos de Europa Formation (Northern Spain; Bahamonde et al. 2007), the Jurassic buildups of the Czorsztyn mounds, (Slovakia; Aubrecht et al. 2002), and the Brocatello Unit (Switzerland; Wiedenmayer 1963; Neuweiler and Bernoulli 2005a, 2005b). These examples show general qualitative estimates of oceanographic regime and paleo-water depth. However, quantitative bathymetric estimates of the depositional environments are lacking, and often the paleoceanographic context, in which red carbonates develop, remains uncertain.

Red staining of carbonate sediments occurs in shallow marine, slope and (hemi) pelagic environments. In permanently submerged marine environments, red staining of carbonates requires: (1) the presence of Fe^{2+}

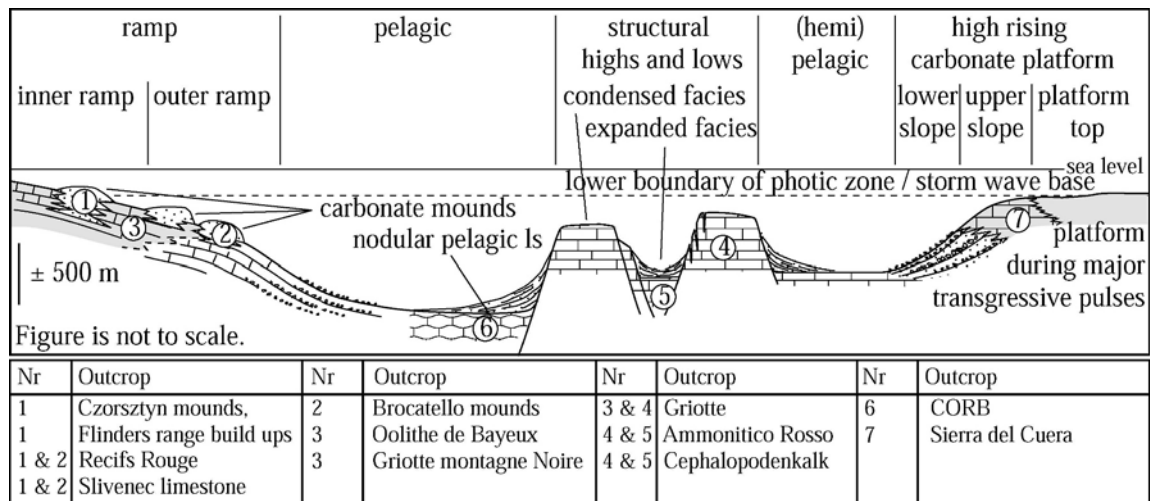


FIG. 1.—Schematic overview of submarine red carbonate depositional environments and facies.

in either seawater and/or sediment, and (2) a mechanism for syngenetic or early diagenetic iron oxidation and pigmentation of carbonates (Haese 2000). The main sources for iron in ocean water are through submarine hydrothermal activity, via riverine influx (Haese 2000), and transport as airborne dust (Donaghay 1991) derived mainly from arid regions.

Mechanisms for sediment pigmentation and iron oxidation are generally complex (Haese 2000) but can be subdivided into: (1) abiotic iron oxidation in combination with well oxygenated water masses and very slow sedimentation rates (Jenkyns 1974), and (2) microbiologically induced iron oxidation (Mamet and Preat 2006 and references therein). This latter mechanism is increasingly well understood and reported from many red carbonates (Bourque and Boulvain 1993; Mamet et al. 1997; Preat et al. 1999; Preat et al. 2000; Preat et al. 2006; Boulvain et al. 2001; Mamet and Preat 2006).

Here, the results of a multidisciplinary study from a Pennsylvanian (Bashkirian–Moscovian, 317 to approximately 309 Ma) carbonate platform exposed in the Sierra de Cuera in northern Spain (Fig. 2; Colmenero et al. 1993; Bahamonde et al. 1997; Della Porta et al. 2002; Della Porta et al. 2003; Della Porta et al. 2004; Kenter et al. 2003; Kenter et al. 2005) are documented and discussed in a process-oriented manner. The focus is on red intervals which crop out on both the platform top and in the slope environment. Structural rotation of approximately 90 degrees, to near vertical, has exposed the full range of carbonate environments ranging from platform top to toe of slope (Fig. 3). The resulting exposure allows sedimentological data to be placed in their bathymetric context (Della Porta et al. 2004; Bahamonde et al. 2007). This study has the following goals: first, to document the facies of the red-stained carbonates in a sedimentologic context; second, to assess the mechanisms and timing of red staining; third, to evaluate the cyclostratigraphic and sequence stratigraphic framework of red-interval deposits; and fourth, to place these findings in a paleoceanographic and bathymetric context.

GEOLOGIC AND STRATIGRAPHIC SETTING

The Cantabrian Zone comprises the northeastern part of the Hercynian orogen in the Iberian massif (Fig. 2; Julivert 1971). During the early Pennsylvanian (Bashkirian–Moscovian; 322–300 Ma), the Cantabrian Zone consisted of a marine foreland basin on which an extensive carbonate platform nucleated (Colmenero et al. 1993; Bahamonde et al.

2007). One of the external flanks of this platform is presently exposed in the Sierra del Cuera range (Fig. 2).

Two distinct carbonate-platform successions are recognized: the Valdeteja and Picos de Europa formations (Fig. 3). In the Sierra del Cuera, the Valdeteja Formation has a predominantly progradational geometry; the overlying Picos de Europa Formation is predominantly aggradational (Bahamonde et al. 1997; Kenter et al. 2003).

During the Moscovian–Ghezelian, the Picos de Europa and Ponga nappes (Fig. 2) were deformed under Varsican compression into a set of imbricate thrust sheets with a nearly vertical orientation. The internal structure of the Sierra del Cuera platform has been preserved and early cementation of platform and slope sediments has minimized the effects of compaction. This allows direct calculations of paleo-water depth.

Five physiographic zones are distinguished within the Sierra del Cuera platform, including the inner and outer platform, upper slope, lower slope, and toe of slope to basin (Fig. 3; Bahamonde et al. 1997; Kenter et al. 2003; Della Porta et al. 2004). The inner platform (Fig. 3) is composed of stacked cycles (5–12 m) which represent shoaling from sub-wave base to well above effective wave base, and are locally overprinted by meteoric diagenetic features (Immenhauser et al. 2002; Immenhauser et al. 2003). The transgressive deposits include algal–peloidal–intraclastic packstones and crinoid grainstones overlain by restricted lagoonal deposits characterized by wackestones and packstones. Cycle-top facies is composed of oncoidal, coated-grain, and ooidal grainstone facies (Della Porta et al. 2002).

The outer platform (Fig. 3) is dominated by bivalve–crinoid grainstones to rudstones. These alternate with thin intervals of bioclastic grainstone, locally with microbial micrite or automicrite (*in situ* precipitated micrite), and radial fibrous cements (Bahamonde et al. 1997; Della Porta et al. 2004).

The platform break grades into a planar upper slope and a slightly concave lower slope (Fig. 3). Upper-slope angles are between 26 and 35° for the Bashkirian strata and up to 42° for the Moscovian (Della Porta et al. 2003). The upper slope, from 0 to approximately 350 meters below the platform break (Fig. 3), is dominated by *in situ* microbial boundstone with calcareous algae, bryozoans, automicrite (*in situ* precipitated micrite) and large voids filled with botryoidal and radial fibrous cement (Della Porta et al. 2003; Bahamonde et al. 2004). The lower slope, between 350 and 800 below the platform break (Fig. 3), is dominated by clast-supported breccia tongues with mostly upper-slope-derived boundstone

TABLE 1.— *Review of red-stained carbonate facies.*

Age	Name	Locality	Dominating lithology	Depositional environment	Red staining mechanism
Lower Cambrian	Carbonate buildups in the Flinders Ranges	Southern Australia	Calcareous, stromatolites; White <i>Epiphyton</i>	Shallow water, high-energy setting; or deeper water, low energy	Red pigmentation is not discussed
Devonian	Slivenec Limestone	Czech Republic	Archaeocyath lime mudstone	Shallow, marine, around the storm wave base	Iron oxidation by iron bacteria
Lower Devonian–Mississippian	Cephalopodenkalk	Rheinisches schiefergebirge; Harz Mountains, Germany	Brachiopod–bryozoan–“tentaculites” grainstones and spiculitic wackestone	<i>Schweller</i> facies: Submarine high, pelagic, open marine. <i>Becken</i> facies: basins adjacent to highs. Submerged reefs, volcanic extrusions, fault blocks	Hydrothermal hematitic enrichment upon volcanic ridges
Lower Devonian	“Mounds” Récifis rouges	Ardennes, Belgium	<i>Schweller</i> facies: Pelagic limestones locally rich in ammonites. <i>Becken</i> facies: silty shales: ostracods and packstone with microbial bindstone	From below storm wave base and photic zone into the fair-weather wave base and photic zone	Detrital Fe origin and abiotic oxidation or Iron oxidation by iron bacteria
Middle–Upper Devonian	Griottes in the Montagne Noire	Montagne Noire, France	Spiculitic wackestone; stromatolites, crinoid and coral wackestone, wackestone with cyanobacteria, peloids and stromatoporoids, algal–coral–peloid wackestone and packstone with microbial bindstone	Outer ramp, hemipelagic below storm wave base, below the photic zone, and poorly oxygenated	Iron oxidation by iron bacteria
Middle Jurassic	“Mud mound” Czorsztyn Limestone Formation	Pieniny Klippen Belt, Western Carpathians, Slovakia	Radiolarian mudstone; sponge–tentaculite wacke to buffestone; laminated tentaculites–ammonoids–bivalve wackestone to packstone; crinoidal packstone	Shallow marine, continental shelf	Red pigmentation is not discussed
Middle Jurassic	Oolithe Ferrugineuse de Bayeux	Normandy, France	Mound: Crinoidal packstones with or without quartz grains, bryozoans, ostracods, pelecypods, brachiopods, agglutinating foraminifera; overlain by pink-red-yellowish mudstone to packstone & grainstone with stromatolite cavities	Distal carbonate ramp, below the photic zone, and below or near storm wave base, low concentration of free oxygen	Iron oxidation by iron bacteria
Upper Jurassic	Mounds in Brocatello Unit	Southern Alps in Arzo, Switzerland	Oncoid rudstones, ooid bioclastic packstone and silted, burrowed wackestone to packstone	Normal marine, subphotic, oxic conditions; deeper water	Red pigmentation is not discussed
Lower Permian–Lower Cretaceous	Ammonitico Rosso, “condensed facies”	Various locations, within the Tethys realm	Fine grained texture, <i>in situ</i> calcified sponges, stromatolites	Structural high and low on submerged carbonate platforms (hemi) pelagic	
Cretaceous	Cretaceous oceanic red beds CORB		Ammonitico Rosso: nodular muddy, marly partings, thin limestone beds. Condensed facies: Fe and Mn crusts, hardground surfaces. Both: ammonites, belemnites, thin-shelled bivalves, and small gastropods	Around CCD in (hemi) pelagic, oxic conditions	Change in redox conditions: Abiotic

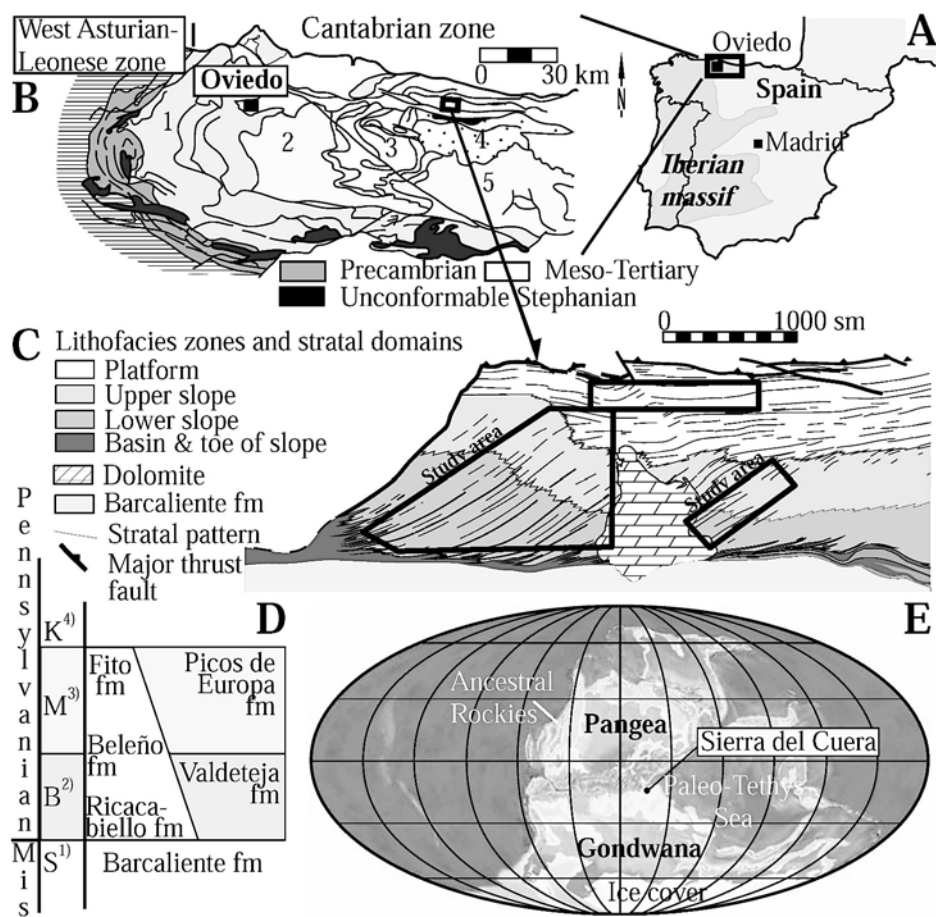


FIG. 2.—A) Overview map of Spain and study area. B) Geotectonic map of the Cantabrian Zone with major tectonic units (after Bahamonde et al. 1997). 1, Fold and Nappe unit; 2, Central Asturian Coal Basin Unit; 3, Ponga Nappe Unit (study area); 4, Picos de Europa Unit; 5, Pisuerga-Carrion Unit. C) Map view of Sierra del Cuera platform (after Kenter et al. 2003) and study windows. D) Chronostratigraphic organization of Ponga Nappe Unit (S = Serpukovian, B = Bashkirian, M = Moscovian, K = Kashimovian). The Sierra del Cuera platform is built by the Valdeteja and Picos de Europa formations. E) Pennsylvanian (310 Ma) world showing location of study area (source map: <http://jan.ucc.nau.edu>).

clasts bound by radial fibrous cement. Towards the base of the lower slope, mud-supported breccias are present (Fig. 3).

At the toe of slope and proximal basin, 800 meters below the platform break (Fig. 3), clast-supported breccia tongues, mud- to clast-supported breccias, and rare platform-derived grainstone alternate with hemipelagic argillaceous lime mudstone with sponge spicules (Bahamonde et al. 1997).

METHODS AND CARBONATE MATERIALS

Section Logging and Field Sampling

The sampling approach used in this study involved two densely sampled transects across the shelf break to the toe of slope, tracing specific red intervals. Each transect represents a time line along the paleoslope (T.R.L-A and B in Fig. 3). In order to establish a sequence-stratigraphic framework, six stratigraphic sections connecting two red intervals were logged perpendicular to these transects at 1:50 or 1:100 scale (S.1 to S.6; Fig. 3). Six shorter sections were logged in 1:25 and 1:50 scale to capture the internal facies organization of red intervals (S.7 to S.12; Fig. 3). Six hundred and seventy samples from the red-stained and the grayish, underlying and overlying facies were collected for thin-section and polished-slab analysis as well as for geochemical analysis. The paleo-water depth of the collected samples are calculated from the distance to the platform break along the bedding surface and the slope angle.

Laboratory Analyses

Petrography.—One hundred and sixty five thin sections and thirty-two polished slabs were analyzed for facies and carbonate petrography

and quantification of the main constituents. Microfossils, macrofossils, and different calcite cement phases were identified, and the relative abundances of major constituents and the characteristics of the internal cavities occluded by early marine to burial cement phases were determined. Quantification of carbonate cements, micrite, and main constituents was undertaken using digitized images of polished slabs.

Cathodoluminescence microscopy was conducted with cold-stage cathodoluminescence operating under 10 to 16 kV accelerating voltage, 380–500 μ A beam current, and a beam diameter of 4 mm. The textural preservation of brachiopod shells is reported in Immenhauser et al. (2002).

Geochemical Analysis.—Three different carbonate materials were analyzed for carbon and oxygen isotope ratios: (1) bulk matrix micrites (both detrital micrite and automicrite); (2) *in situ*, well-preserved brachiopod shells; and (3) early-marine (fibrous) cements. Samples of matrix micrite and (marine) fibrous cement were collected from polished or cut slabs to avoid weathered surfaces and large bioclasts, using a hand-held drill with 1 mm diameter drill bits. Brachiopod shell and a number of carbonate-cement subsamples were collected using a computer-steered Micromill[®] as described in Dettman and Lohmann (1995). Carbonate-cement and brachiopod-shell subsamples were analyzed on a Thermo Finnigan MAT 252 isotope ratio mass spectrometer at the Vrije Universiteit in Amsterdam, The Netherlands. Repeated analyses of carbonate standards show a reproducibility of better than 0.1‰ for $\delta^{18}\text{O}$ and 0.05‰ for $\delta^{13}\text{C}$. Matrix micrite samples (approximately 0.1 mg) were analyzed on a Thermo Finnigan Delta^{Plus} GasBench II at the Vrije Universiteit in Amsterdam, The Netherlands, and on a Finnigan Delta^S

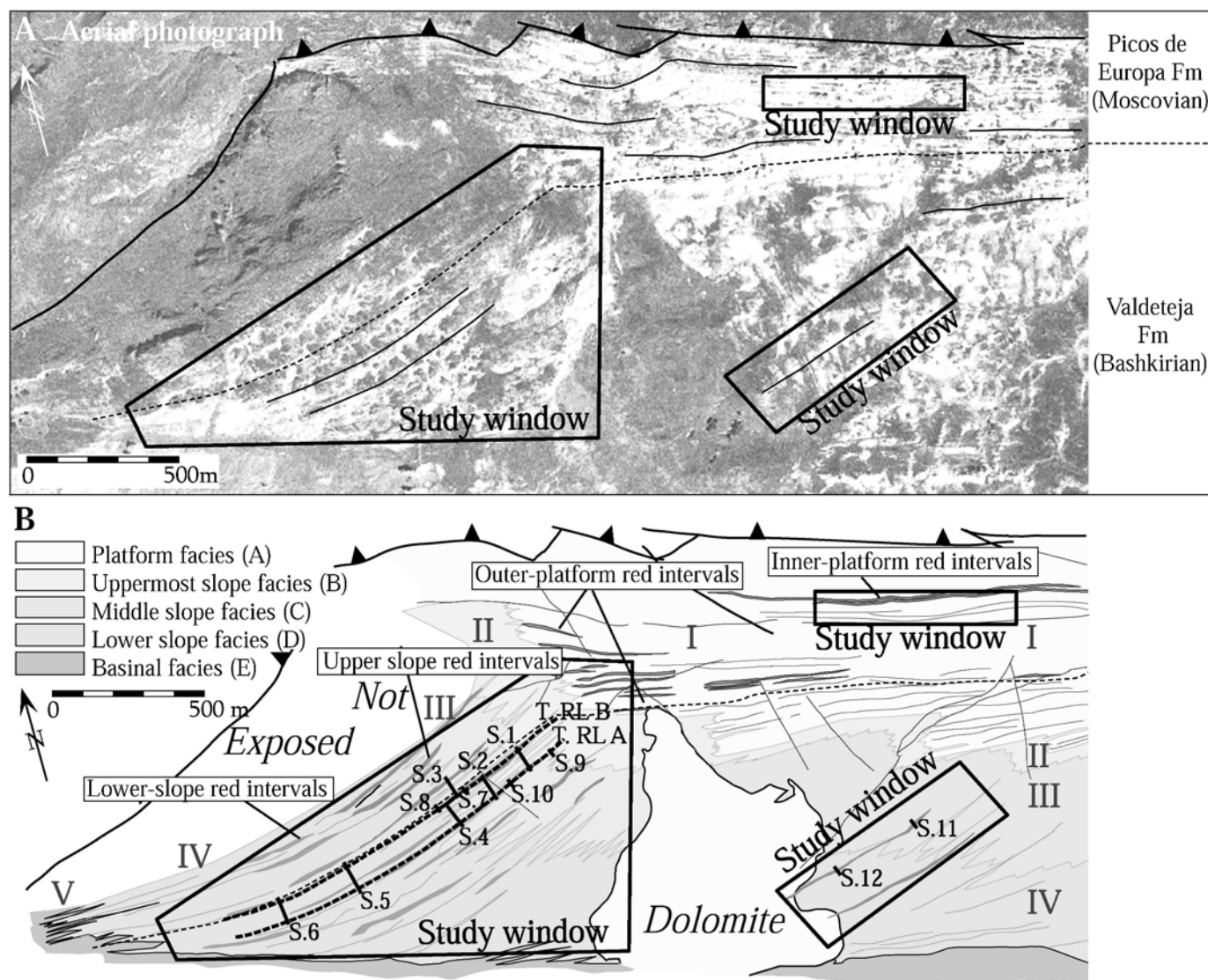


FIG. 3.—A) Aerial photograph of the Sierra del Cuera external flank showing study areas. B) Schematic overview of physiographic domains on the Sierra del Cuera platform. I) Platform; II) Uppermost slope; III) Upper to middle slope; IV) Lower slope; and V) Toe of slope (Figs. 5, 11). Frames indicate study areas, and black lines refer to the measured transects (dotted; T.R.L A and B) and sections (S.1–12).

GasBench II at the Ruhr University, Bochum, Germany. Reproducibility is ± 0.1 and $\pm 0.2\%$ for carbon and oxygen respectively.

Samples of marine fibrous cement were analyzed for Ca, Mg, Sr, Mn, and Fe elemental concentrations in order to detect alteration during burial diagenesis. Samples of matrix micrite were analyzed for Fe elemental concentrations. Samples were dissolved in 1M HCl and centrifuged to separate the Fe in the calcium carbonate from that attached to clay minerals. Elemental compositions were measured by inductively coupled plasma-atomic emission spectrometry (ICP-AES). The resulting analytical precision of repeated analyses is in the order of $\pm 1.5\%$ for Ca and $\pm 8\%$ for Mg, Sr, Mn, and Fe.

SEDIMENTOLOGY AND BIOTA OF RED INTERVALS

A total of seven red intervals are present on the slope of the Sierra del Cuera. Two red intervals (each 5 meters thick) are present in the Bashkirian (progradational) slope and have tabular geometries. Five red intervals with a lenticular to tabular geometry and a maximum thickness of 30 meters occur in the Moscovian aggradational slope (Fig. 4). Upper-

slope red intervals commence generally between 80 and 200 meters below the platform break and extend downslope to 450 meters (Fig. 3, 5, 6; Della Porta et al. 2003; Bahamonde et al. 2004). They are composed of reddish, muddy or peloidal patches or well-developed layers, rich in organic material and characterized by an elevated clay content in the matrix micrite with respect to underlying and overlying sediments. Pore spaces, cavities, and surfaces are occluded by radiaxial fibrous calcite cement forming cementstones (*sensu* Webb, 1996; Fig. 6, 7, 8). Although marine cements are volumetrically abundant throughout the slope of the Sierra del Cuera, biocementstones are linked exclusively to red-stained intervals. Lower-slope red intervals are composed of redeposited sediments forming the matrix in rudstones and breccias (Fig. 6, 7). Seven main facies types are recognized and are summarized in Table 2 and Figure 5.

Modes of Red-Interval Sedimentation

Three modes of red-interval sedimentation are recognized: (1) episodic, high-depositional-rate sedimentation; (2) slow, continuous sedimentation;

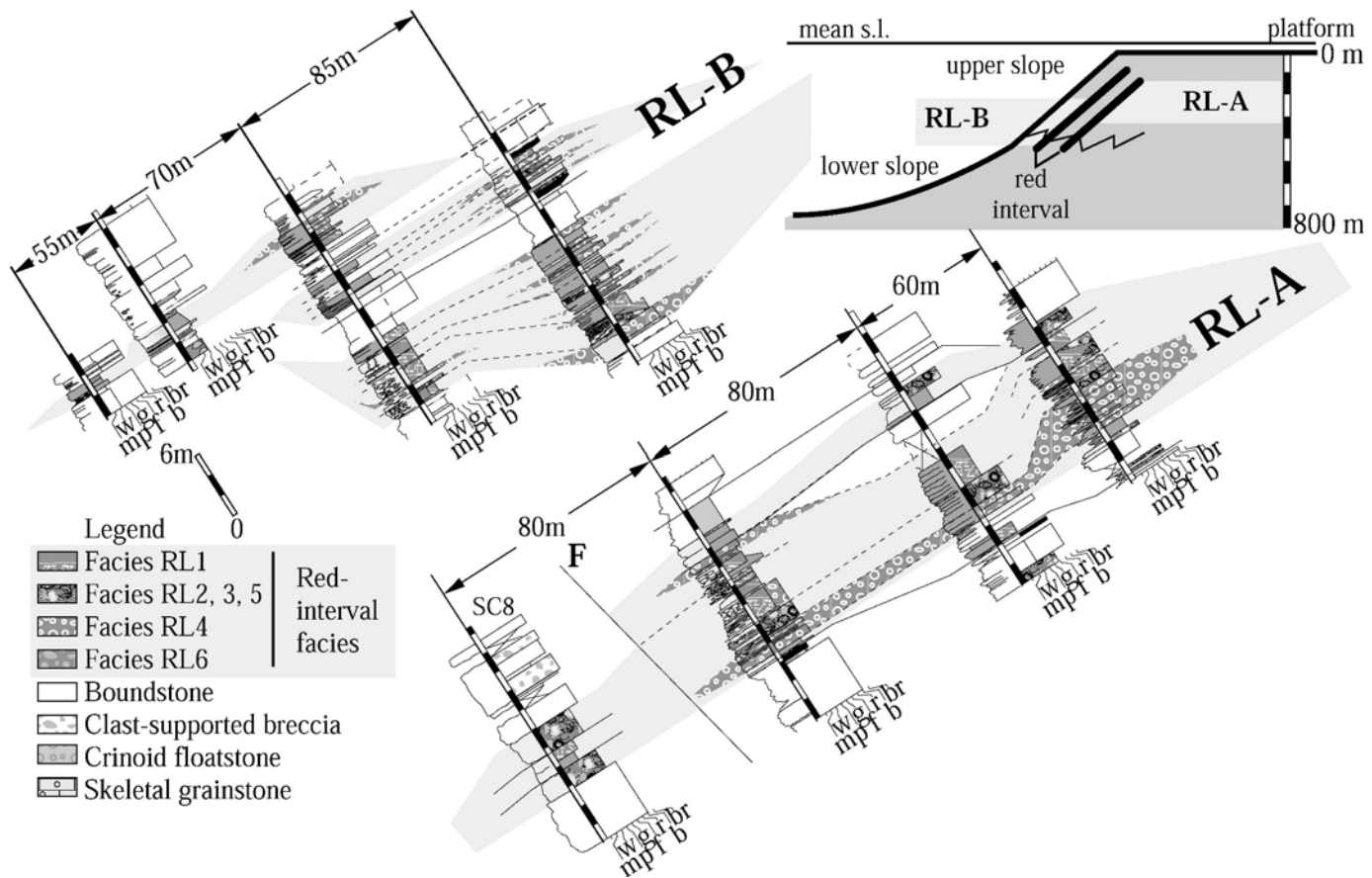


FIG. 4.—Cross section of red-interval facies organization on the upper and middle slope. Red intervals RL-A and RL-B show downslope-decreasing abundance of crinoid floatstone (RL3) and biocementstone facies and increasing skeletal wackestone and packstone facies (RL1). RL-A is built by one coherent interval whereas RL-B is built of three subsequent packages.

and (3) reduced to non-sedimentation (omission). Arguments for this distinction are based on the interpretation of lithofacies types, sedimentological features, and biotic associations in red intervals.

Lithofacies RL4 (crinoid floatstone facies; Fig. 7) and RL6 and 7 (red-matrix breccia and toe-of-slope red wackestones to mudstone; Fig. 6) represent fast, episodic sediment deposition. The paleo-habitat of crinoids in the Sierra del Cuera carbonate platform was located on the wave-swept platform top, where they were disintegrated, transported, and accumu-

lated into bioclastic bars during transgressive events (Della Porta et al. 2004). On the slope, crinoids form isolated lens-shaped carbonate bodies (Lithofacies RL4; Fig. 4) interpreted as calciturbiditic deposits on the basis of typical gravity-flow features. Calciturbidite deposits represent episodic events transporting crinoids downslope from the platform top. The large volumes of crinoid hash (i.e., calciturbidites) are common features of Paleozoic carbonate platforms during transgressive pulses (Immenhauser et al. 2003; Bahamonde et al. 2004; Della Porta et al. 2004). The matrix of RL6 and facies RL7 consist of redeposition products of the upper-slope red-interval deposits. Typical gravity-flow features such as normal grading and slump structures in matrix wackestone of RL6 and RL7, respectively, are interpreted as the result of fast sedimentation.

Lithofacies RL1 (Fig. 6, 7) is the dominant red-interval facies of the upper slope, reflecting slow but continuous sedimentation. This is indicated by extensive bioturbation (incipient condensation) and a high but not dominant proportion of skeletal material relative to the micritic matrix. The absence of hardground surfaces suggests that sedimentation was not interrupted.

Bryozoan and brachiopod cementstone and biocementstone (RL2, 3, 5; Fig. 6) represent modes of considerably reduced sedimentation or omission. Bryozoans and brachiopods require firm substrates (Clarkson 1996). Minor reworked or *in situ* brachiopods or bryozoans are encased in marine cements, forming bryozoan or brachiopod cementstones (Figs. 7, 8; Martinez Chacon and Bahamonde 2005). Biocementstones originate from skeletal remains which accumulated over time to skeletal lenses and

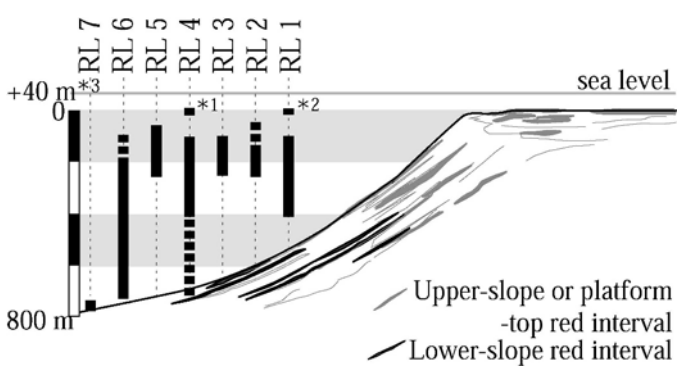


FIG. 5.—Schematic overview of bathymetric distribution of red carbonate facies on the Sierra del Cuera platform and slope. For key to facies see text (RL). *1 = RL4 facies on the outer platform. *2 = RL1 facies in the inner platform. *3 = sea-level maximum following Maynard and Leeder (1992; 40 m).

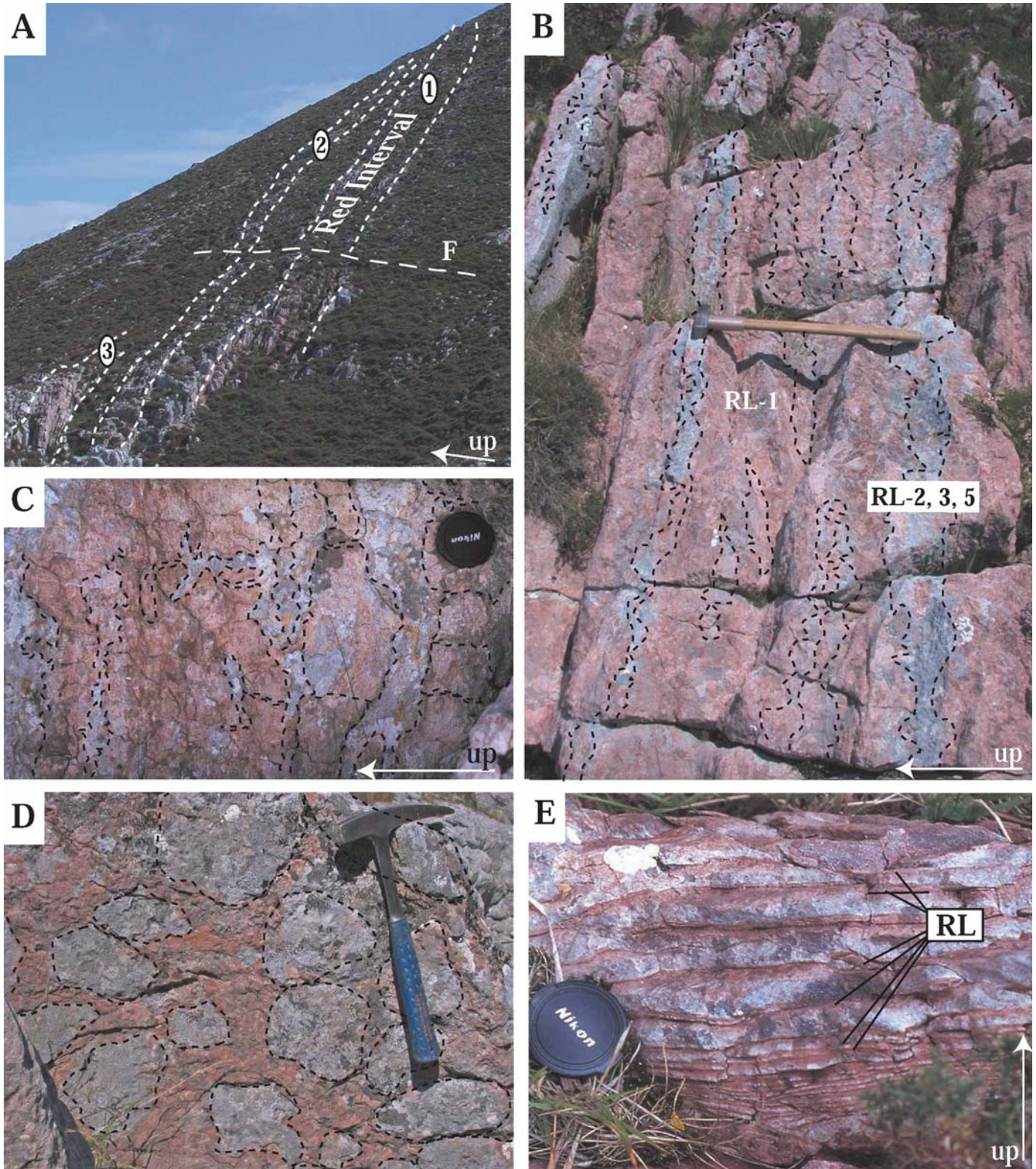


FIG. 6.—Outcrop photographs of red intervals. Arrows indicate stratigraphic up in all images (A–E). **A)** Overview image of upper slope red-stained interval (RL-B in Fig. 5) composed of three successions (1–3). Fault is indicated with F. Platform break is towards the upper right. **B)** Meter-scale overview of upper-slope red interval, showing irregular alternation of red-mud-supported (RL1, 3, 4) and biocementstone facies (RL5). Hammer is 60 cm long. **C)** Detail of red wackestone to packstone (facies RL1) with fractures and cavities filled with radiaxial fibrous calcite and RL2 facies. Diameter of lens cap is 55 mm. **D)** Plan view of red-interval mud-supported breccia. **E)** Toe-of-slope laminated red-interval mudstone (RL) alternating with grayish basinal facies. Diameter of lens cap is 55 mm.

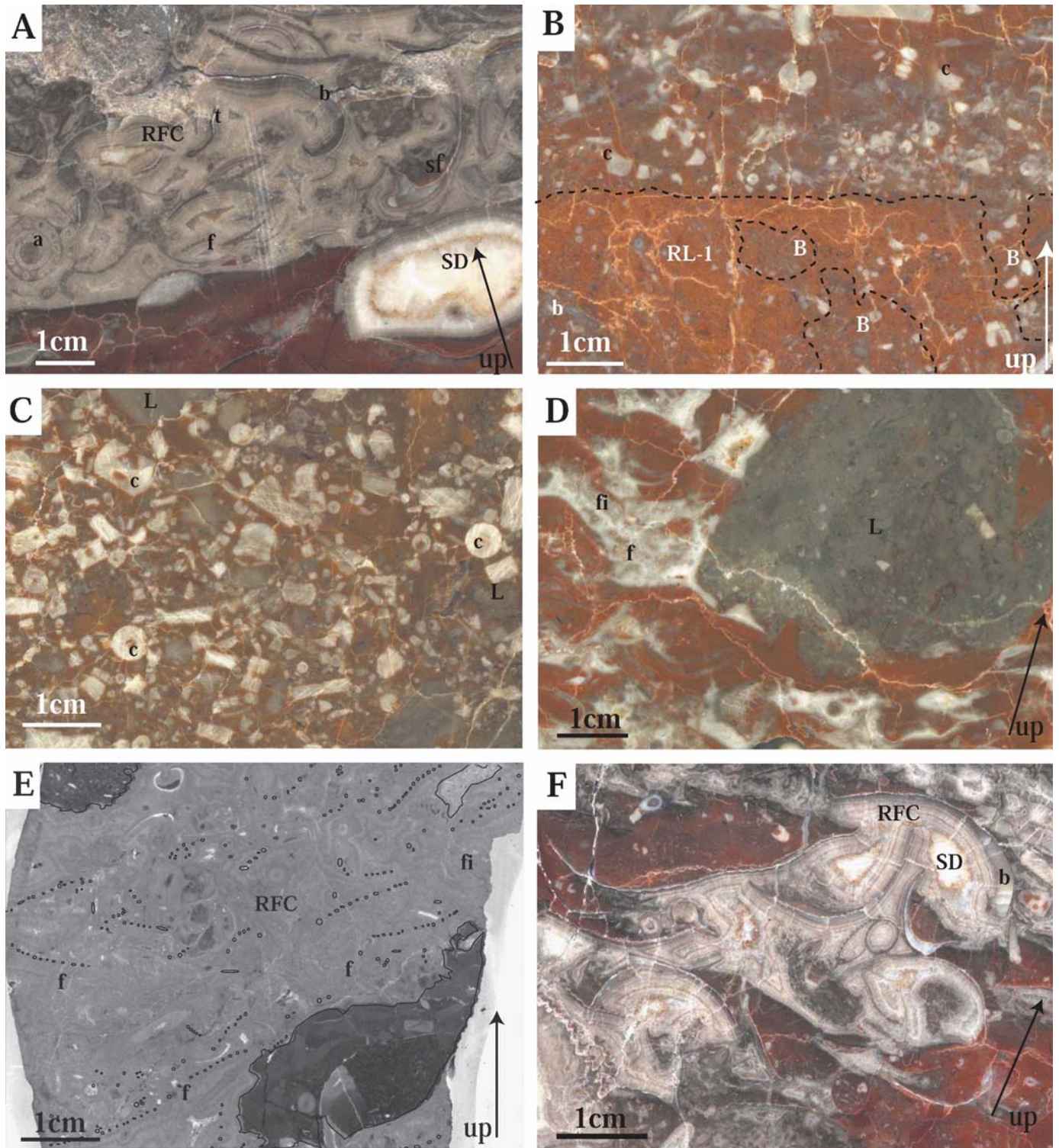


FIG. 7.— Polished slabs. **A)** RL5 biocementstone facies overlying red-stained muddy facies (RL1). Typical deeper-water association of biota: Brachiopods (b), ammonoids (a), trilobite fragment (t), fenestellid bryozoan (f) occluded by radial and radiaxial fibrous cement (RFC). Remaining pore space is filled with saddle dolomite (SD) and internal sediment (SF). **B)** Crinoid-rich facies (c; RL4) overlying bioturbated facies (RL1), note burrows (B). **C)** Crinoid floatstone facies (RL4), note lithoclasts (L). **D)** Red-mud-supported breccia. Lithoclast is microbial boundstone. Matrix shows shelter cavities filled with rfc. Note fistuliporid bryozoan (fi) encrusting cavity wall and fenestellid bryozoan (f) inhabiting the cavity. **E)** Bryozoan biocementstone. *In situ* fenestellid bryozoans (f) fringed by multiple isopachous rims of RFC. Other bioclasts include fistuliporid bryozoa (fi), crinoid ossicles (c), brachiopod shells (b), and gastropods (g). **F)** Primary (shelter) porosity in bioclastic wackestone (RL1) filled with RFC and saddle dolomite (SD). Arrow indicates stratigraphic up in all images (A–F).

TABLE 2.— Schematic overview of red-interval lithofacies types.

Texture and matrix	Cements	Biotic association	Porosity, ichnofacies, sedimentary structures	Bathymetric range*1	Red staining
Wackestone to packstone; micrite or microsparite	Isopachous rims of radialial fibrous, scalenohedral calcite (growing directly from the walls of vuggy cavities), equant mosaic calcite and saddle dolomite	RL1: Bioclastic wackestone packstone facies (Fig. 6B, 7B, 8C, and E) Fenestellid, fistuliporid, cryptostomate bryozoans, brachiopods. Additionally: Crinoid ossicles, ammonoids, gastropods, pelecypods (thin-shelled bivalves), ostracods, sponge spicules, trilobites, rugose corals, <i>Donezella</i> algal fragments Foraminifera: <i>Tuberitina</i> , <i>Tetrataxis</i> , <i>Tubiphytes</i> (<i>Shanovella</i> ?; Riding, 1992), fusulimids, <i>Palaeotextularia</i> , <i>Hemigordius</i>	Cavities, shelter, framework, intragranular porosity, rare stromatactis-like voids, vuggy, fracture, moldic porosity, and washed burrows	Inner-platform domain and slope: 80–450 m	Various intensities of brown-reddish to intense dark red staining
Cementstone, internal micritic sediment	Radialial fibrous calcite, scalenohedral overgrowth cement, equant mosaic calcite, saddle dolomite	RL2: Bryozoan cementstone facies (Fig. 6B, 7E, 8F) Fenestellid bryozoans. Additionally: Crinoid ossicles, brachiopod shells, fusulimids and <i>Tubiphytes</i>	Facies is present in cm to dm-sized irregular -shaped cavities	Upper slope: 0–200 m	Internal sediment is weakly to intensely stained
Cementstone, internal micritic sediment	Radialial fibrous calcite, scalenohedral overgrowth cement, equant mosaic calcite, saddle dolomite	RL3: Brachiopod lithosome facies*2 Productida, Spiriferida, Orthida, Rhynchonellida, Terebratulida, Orthotetida, Spiriferinida	Not applicable	Upper slope: 0 to 200 m	Not stained or various intensities of red staining
Packstone–floatstone; micrite	Not applicable	RL4: Crinoid floatstone facies (Fig. 7B, C) Crinoid ossicles. Additionally: fistuliporid bryozoans, gastropod and pelecypod shell debris, productid brachiopods, ostracods, and <i>Palaeotextularia</i> foraminifera	Not applicable	Upper slope and middle slope: 0–300 m	Internal sediment is weakly to intensely stained
Cementstone, internal micritic sediment	Isopachous rims of radial and radialial fibrous calcite, blocky calcite, or saddle dolomite	RL5: Biocementstone facies (Fig. 6B, 7A, F) Brachiopod shells, fenestellid, fistuliporid bryozoans, crinoid ossicles, and, less common ammonoids, trilobites, and solitary corals, sponge spicules, thin-shelled bivalves	Not applicable	Upper slope and middle slope: 0–300 m	Internal sediment is weakly to intensely stained
Breccia: Upper-slope-derived boundstone lithoclasts, red-stained wackestone matrix	Radialial fibrous calcite, scalenohedral overgrowth cement and blocky calcite	RL6: Red-mud-supported breccia facies (Fig. 6D, 7D) Debris of bryozoans, brachiopods (and spines), pelecypod fragments, ostracods, crinoids, and rare trilobites, common <i>Tubiphytes</i> , rare sessile foraminifera (e.g., calcitonellids)	Shelter porosity; matrix sediments are sometimes graded	Upper slope to lower slope: 200 to 700 m	Matrix micrites are often dark-red stained
Red and gray, laminated mudstones and wackestones; micrite, silt	Not applicable	RL7: Toe-of-slope red facies (Fig. 6E) Few undifferentiated bioclasts	Slumping and sliding features	Lowermost slope to toe-of-slope: 700–800 m	Laminae are stained red

*1) Depth is measured with reference to platform break

*2) Brachiopod determination, see Martínez Chacon and Bahamonde (2005)

layers of many centimeters to a few decimeters thick. Within the pores and cavities of these debris layers, marine fibrous cements nucleated on skeletal grains and occluded most of the pore space (Bahamonde et al. 2004), resulting in early marine lithification. Perhaps due to very low sedimentation rates or because of current activity, very little carbonate micrite was washed into the system.

Sequence Stratigraphic Significance of Red Intervals

The quantitative approach to platform geometry and paleo-water depth as applied in this study allows for a sequence-stratigraphic interpretation of red intervals within their bathymetric framework. This is of significance for the interpretation of red carbonate facies in general, and is probably applicable to other exposures in comparable settings and of similar age where a similar bathymetric control is lacking.

The lithofacies of red intervals are indicative of a deeper-water environment with respect to the underlying and overlying strata and hence are considered as evidence for maximum water depth of the platform top and slope. This is suggested by the presence of a largely light-independent (heterotrophic) biotic association in red intervals on the inner platform (mainly bryozoans, brachiopods, ostracods, and crinoids; Facies type RL1) and the outer platform (crinoids, bryozoan debris; facies RL4; Fig. 9). They contrast with the underlying and overlying strata, which are characterized by the presence of a light-dependent (phototrophic) biotic association (e.g., *Donezella*, phylloid algae) or typical shallow-water transgressive deposits such as grainstones with coated grains, pisoids, and intraclasts (Della Porta et al. 2002; Della Porta et al. 2004 for details on platform facies).

On the slope, deepening is suggested by calciturbidites (facies type RL4) within red intervals (Fig. 10) and a faunal assemblage with a more open-water biota (i.e., ammonoids and thin-shelled bivalves; facies types RL1 to 5).

In terms of sequence stratigraphy, the red intervals are interpreted as maximum flooding intervals (mfi; Figs. 9, 10). Use of the term “interval” as opposed to the more conventional “maximum flooding surface” (mfs) of sequence stratigraphic nomenclature reflects the difficulty of identifying one specific surface of maximum flooding (Figs. 9, 10; Elrick and Read 1991).

The uppermost Bashkirian and lower Moscovian highstand on the Sierra del Cuera platform was characterized by a prograding and prograding-aggrading platform development (Della Porta et al. 2004). Upper-slope and middle-slope settings were dominated by microbial boundstones. Clast-supported breccia was shed basinwards onto the mid-slope. This was perhaps the result of platform-slope readjustment, taking into account the slope angles of up to 42°, at the angle of repose (Kenter 1990). On the lower slope, clast-supported breccia alternates with thin beds of red-mud-supported breccia. The deposition of breccia beds with a red matrix was probably due to redeposition of the upper-slope and mid-slope-red-interval sediments.

Sequence boundaries are defined on the outer platform as the change from ooidal (in the Bashkirian) and coated-grain-dominated deposits to a facies dominated by intraclasts, oncoids, and crinoids (transgressive surface; Fig. 9). There is no unambiguous geometrical evidence for the presence of a lowstand systems tract (LST) or a falling-stage systems tract on the slope of the Sierra del Cuera. Nevertheless, skeletal grainstone intervals in the lower slope, overlain by a predominantly aggrading platform, are interpreted as lowstand deposits. The sequence-boundary equivalents on the slope of the Sierra del Cuera are tentatively placed at the base of these intervals (Fig. 10).

At the Bashkirian–Moscovian boundary and during the Kashkirian (lower Moscovian), red-stained intervals are present across portions of the inner platform (Fig. 3). They are interpreted as near-drowning events of the Sierra del Cuera platform (Immenhauser et al. 2003). Bahamonde

et al. (1997) and Della Porta (2003) ascribe these events to a combination of maximum flooding and a change in subsidence rate (Fig. 11). Relative rates of tectonic subsidence are assessed from the overall change in platform development at the Bashkirian–Moscovian boundary from prograding to aggrading (Figs. 3, 11; Bahamonde et al. 2007).

Individual red intervals are stratigraphically separated by approximately 130 m of microbial boundstone in the Bashkirian and 50 to 70 m in the Moscovian portions of the slope (Figs. 3, 10). Average accumulation rates of 605 ± 35 m/Myr for the Bashkirian (Langesian–Duckmantian) and 130 ± 5 m/Myr for the Moscovian Sierra del Cuera upper slope were proposed in Della Porta et al. (2004; based on the timescale published in Menning et al. 2006). In contrast, the timescale of Gradstein and Ogg (2004) does not provide sufficient detail on the duration of the upper Bashkirian (6.4 Myr *versus* 8 Myr duration as suggested in Menning et al. 2006). Assuming that the estimates of the accumulation rates are correct, red intervals on average formed every 0.21 Myr during the Bashkirian and between 0.38 and 0.54 Myr during the Moscovian. These values fall in the domain of orbital forcing and in particular the eccentricity frequencies of 100 and 400 kyr.

In this context a comparison of the slope red intervals with the classical cyclothems (Heckel 1986) from the Western Interior Basins of the North American mid-continent is of interest. Cyclothems describe transgressive–regressive stratigraphic sequences as a result of waxing and waning of ice sheets during the Late Pennsylvanian and Permian. Nevertheless, the Western Interior cyclothems are younger (late Moscovian to Ghezelian) than the Bashkirian–Moscovian red-interval cycles on the Sierra del Cuera. Therefore, the direct comparison of the Sierra del Cuera platform slope and the Western Interior is not justified. Subsequent studies by Heckel (1994) and Strasser et al. (2007) show that although obscured by local environmental parameters, cyclothems are most likely related to Milankovitch cycles, in particular the ~ 32 kyr obliquity, or the 100 and 400 kyr eccentricity cycles. It is beyond the scope of this study to investigate these aspects in detail. Nevertheless, when interpreting the Sierra del Cuera cycles, climatic and glacio-eustatic factors and their relation to paleoceanography must be considered.

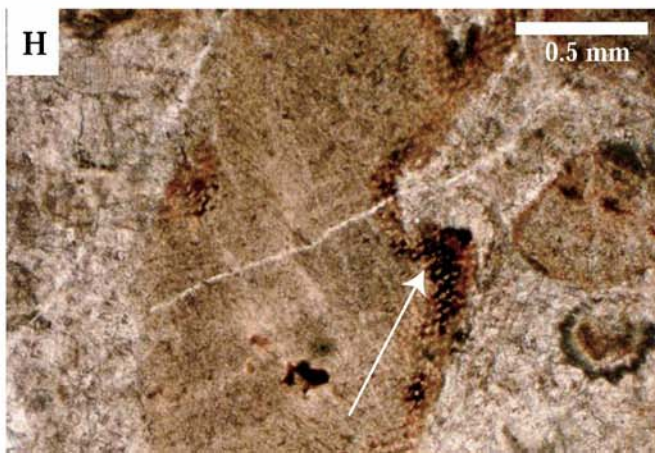
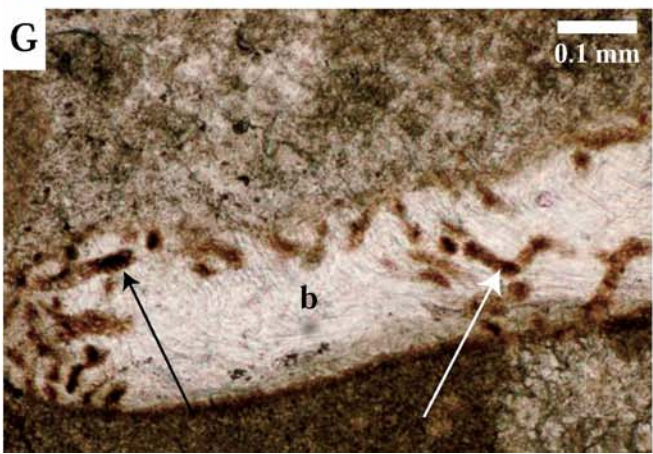
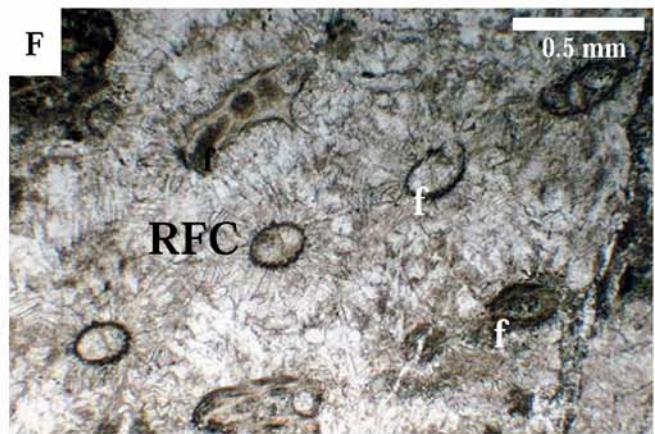
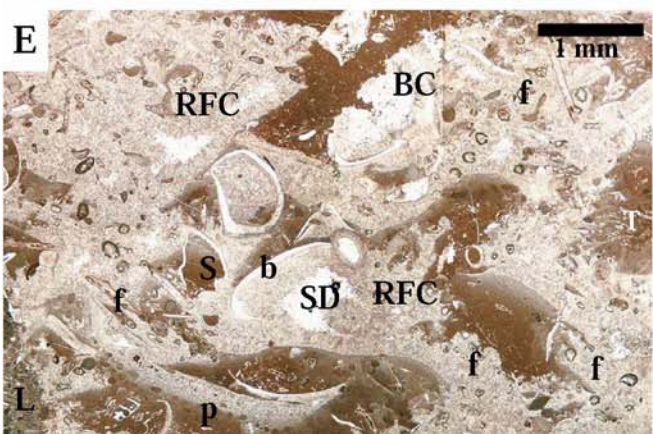
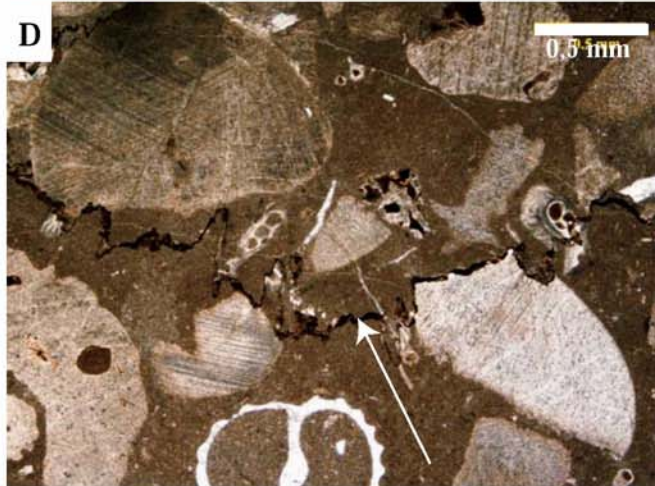
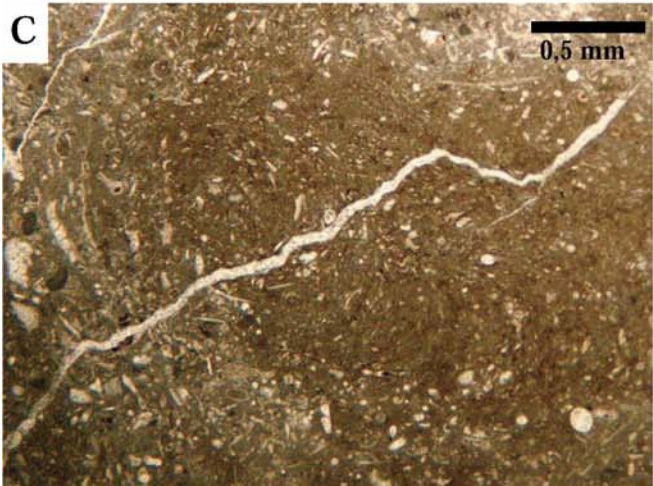
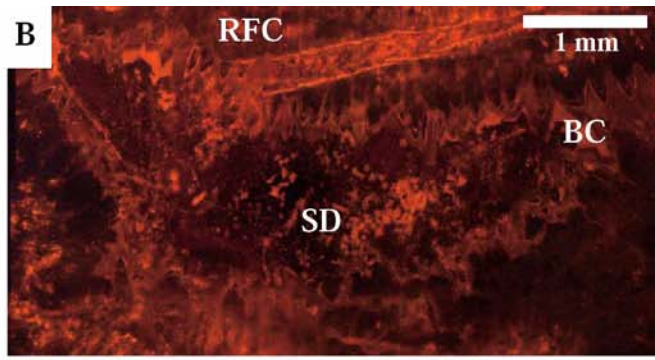
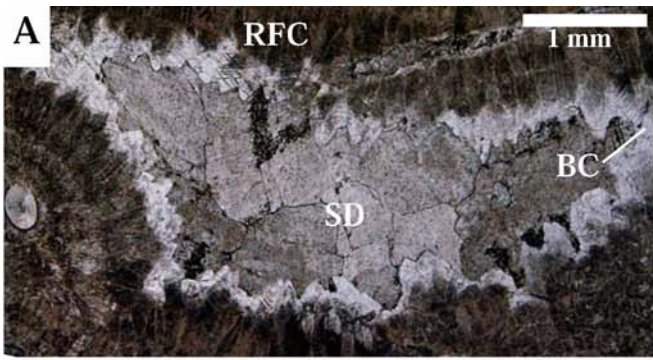
GEOCHEMISTRY OF CARBONATE MATERIALS AND CEMENT PETROGRAPHY

An overview of the carbon- and oxygen-isotope composition of bulk brachiopod shell material and matrix micrites from both slope red intervals and gray boundstone strata is provided in Table 3A and B. Table 3C summarizes the trace-element content of radiaxial fibrous cements, and red and boundstone micrites.

Cement Petrography and Geochemistry

The Sierra del Cuera red-interval limestones reflect a diagenetic history characterized by a long and complex succession of dissolution, precipitation, and fracturing events. It is beyond the scope of this paper to discuss each diagenetic stage in detail. Here, the focus is on the diagenetic stages relevant for the syndepositional and paleoceanographic context of the red intervals, i.e., marine and shallow burial phases as illustrated in Figure 12. Specifically this includes radiaxial fibrous calcite, syntaxial-overgrowth, and scalenohedral calcite precipitation.

Petrography and Geochemistry of Radiaxial Fibrous Calcite.—Radiaxial fibrous calcite (rfc) forms isopachous crusts fringing skeletal frameworks and bioclasts. These cements occlude pore types such as interparticle, shelter, fenestral, cavernous, and breccia porosity and fracture voids (Figs. 7, 12). The spatial and bathymetric distribution of rfc reaches from the platform break to the lower slope independent of the paleo-bathymetric setting. Cement crusts have a composite thickness of 0.1 to




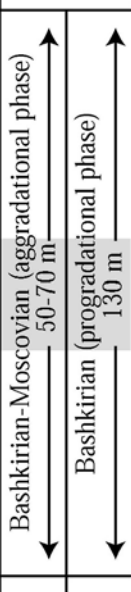
Sequence	Upper-slope thickness	Outer-platform deposits	Slope deposits	
		after Della Porta et al. (2004)	Upper slope (0-350 m)	Lower slope (300-600 m)
		Grainstone with ooids, coated grains, and pisoids.	Alternating beds of mud-supported and clast-supported breccia microbial boundstone and crinoid-dominated grainstone and packstone.	Wackstone-packstone-grainstone with platform-derived components.
		Bashkirian: Skeletal-algal grainstone to packstone with foraminifers and sessile forams. Moscovian: Massive algal wackstone and skeletal wackestone.	Microbial boundstone interbedded with thick to thin levels of clast-supported and few red-mud-supported breccia with upper-slope boundstone clasts.	Clast-supported breccia towards lowermost slope mud-supported and intercalated with few levels of red mud-supported breccia.
		Crinoidal packstone and grainstone forming lens-shaped bioclastic bars. Only uppermost Bashkirian - lower Moscovian intervals.	Red skeletal wackstone and packstone dominated, crinoid floatstone and cementstone with marine fibrous cement.	Breccia: boundstone lithoclasts, red-mud supported. Sediments are deposited lateral to upper-slope red-stained intervals.
		Bashkirian: Skeletal-algal packstone, with alternated with boundstone. Moscovian: Algal rich wackestone with bryozoans, echinoderms, foraminifers.	Microbial boundstone with interbedded thick to thin levels of clast supported and few red mud-supported breccia with upper-slope boundstone clasts.	Clast-supported breccia with upper-slope boundstone clasts. Lowermost slope breccia is mud supported. Lens-shaped bodies of red-mud-supported breccia.
		Coated grain-intraclast-oncoid-ooid grainstone.	Packstone and grainstone with platform-derived material and crinoid-dominated floatstone (thin intervals).	Packstone and grainstone with platform-derived material and boundstone lithoclasts.

FIG. 9.— Schematic overview of latest Bashkirian–early Moscovian depositional cycle. Outer-platform deposits are modified after Della Porta et al. (2004). Interpretation of slope deposits is based on this study and includes data from Bahamonde et al. (2004 and references therein).

3 mm (Fig. 8) and are generally thicker on the upper and middle slope compared to those on the lower slope. Zonation in rfc is marked by a difference in inclusion density or thin layers of internal sediment. Individual zones range in thickness from a few tens to hundreds of micrometers.

Under cathodoluminescence (CL), radiaxial fibrous calcite is commonly non-luminescent with local irregular patches or well-defined zones of brighter luminescence (Fig. 8). The $\delta^{13}\text{C}$ ratio of red-interval rfc (5.1 to 5.7‰; Table 3) is fairly consistent with fibrous cements sampled within the gray boundstone facies of the carbonate slope (4.9 to 5.6‰; Table 3). In contrast, the fibrous-cement $\delta^{18}\text{O}$ values oscillate between -4 and 0.5‰ (Table 3). These values are considerably higher than in radiaxial calcites from underlying and overlying gray boundstones (ranging from -7 to -1‰ ; Fig. 13). This difference is considered to be significant. Manganese and Sr elemental concentrations in the selected radiaxial fibrous calcite samples are low. Strontium concentrations from rfc range between 200 and 500 ppm and Mn concentrations in most rfc samples measured are below 250 ppm. One set of samples, characterized by considerably higher Mn values of more than 400 ppm (Fig. 13C), are considered diagenetically overprinted (Tobin et al. 1996).

Diagenetic Environment.—It has been suggested that radiaxial calcite is an *in situ* alteration product of a former marine high-Mg calcite (e.g.,

Wilson and Dickson 1996) whilst early studies assumed an aragonitic precursor (Bathurst 1977) or primary precipitate (Kendall 1985). Previous work has shown $\delta^{13}\text{C}$ datasets of radiaxial fibrous cements which are in agreement with reconstructed coeval seawater isotopic values of Mississippian oceans (Lees and Miller 1995) and Pennsylvanian oceans (Mii et al. 2001). The $\delta^{13}\text{C}$ ratio of the fibrous cement dataset measured on the paleo-slope of the Sierra del Cuera plots well in the field of predicted Bashkirian–Moscovian open marine seawater according to Bruckschen et al. (1999) (Fig. 14). This is supported by the locally weak and patchy, but predominantly nonluminescent nature of these cements and their low Mn concentrations (< 200 ppm), both of which are indicative of a marine origin (Bruckschen et al. 1999). It is accepted that the fibrous cements underwent high-Mg to low-Mg alteration and diagenetic reequilibration within the shallow-burial marine porewater domain. The geochemical data, however, imply that porewater geochemistry was not markedly different from that of the ambient seawater.

Dissolution Features and Scalenohedral Overgrowth Cement Petrography.—After dissolution of metastable shell materials, scalenohedral calcite was precipitated into biomolds and syntaxially encrusted the radiaxial fibrous cements (Fig. 8A). Scalenohedral calcites are translucent and display uniform extinction under crossed polars. The first scalenohedral precipitates exhibit rare (secondary) inclusions sometimes along

FIG. 8.— Photomicrographs of red-stained facies: **A**) transmitted-light photomicrograph of cavity, filled with radiaxial fibrous calcite (RFC), scalenohedral calcite (SC), blocky calcite (BC), and saddle dolomite (SD). **B**) CL photomicrograph of same cavity. Note patchy luminescence of rfc, the nonluminescent overgrowth scalenohedral calcite and bright–dull luminescent, zoned blocky calcite. Dark to red luminescent saddle dolomite is replacing predominantly blocky calcite. **C**) Burrowed skeletal wackestone. **D**) Crinoid floatstone (RL4) with few additional skeletal fragments of gastropods and bryozoa, crosscut by stylolite (arrow). **E**) Composite photomicrograph of mid-slope red-interval facies type RL1. Primary (enhanced) cavities are filled with internal sediment (S), RFC, blocky calcite (BC), and saddle dolomite (SD). Note the fenestral fronds (f) in cavities, Tetrataxis foraminifera (t), peloids (p), and lithoclast (L). **F**) Photomicrograph of bryozoan cementstone facies RL3 showing fenestral fronds (f) occluded by RFC. **G**) Photomicrograph of a bored brachiopod shell. Borings (arrows) are filled with iron-rich precipitate. **H**) Photomicrograph showing a crinoid ossicle. Primary and dissolution pores are filled with iron-rich precipitate (arrow).

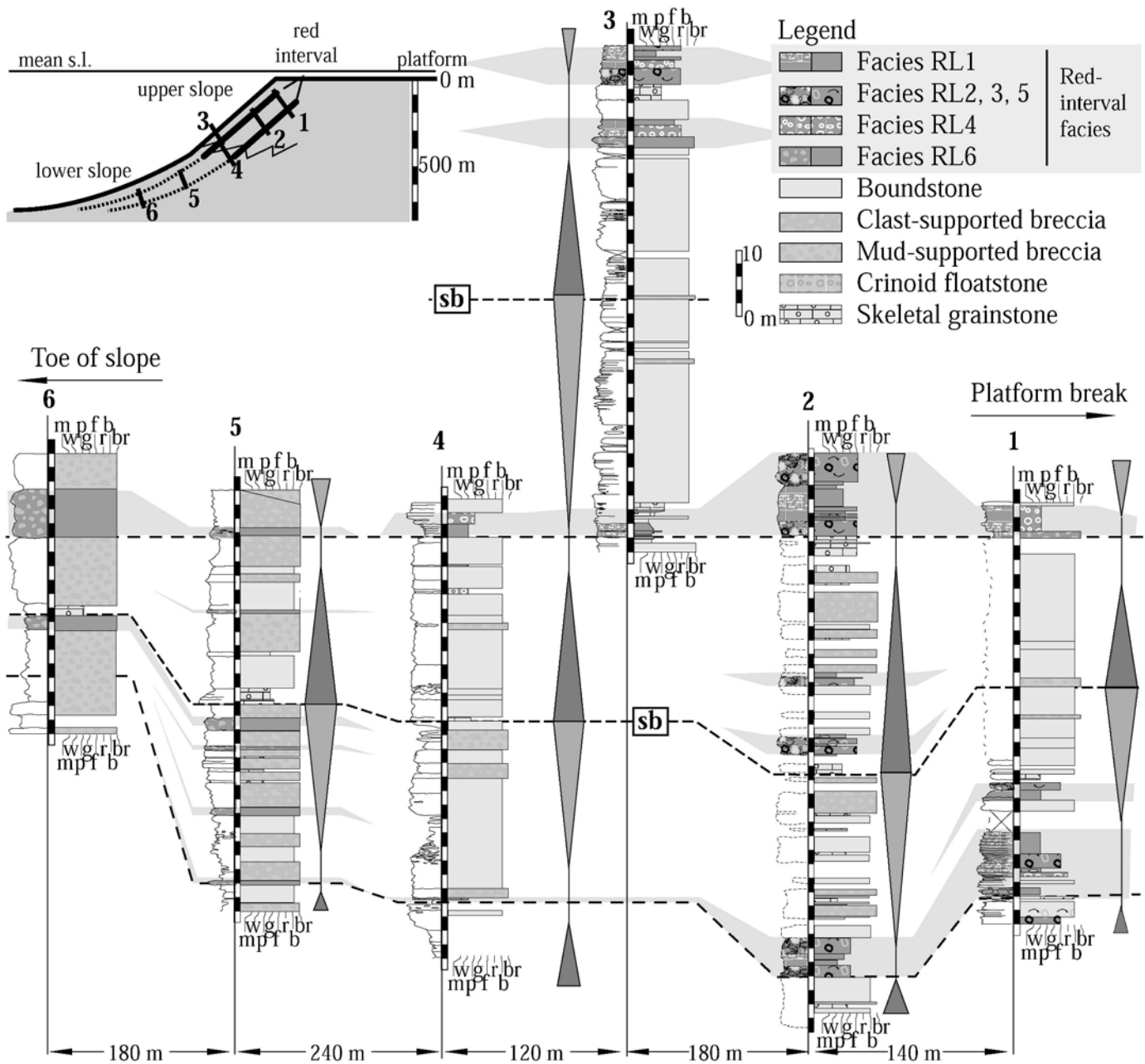


FIG. 10.—Sequence stratigraphic interpretation of early Moscovian Sierra del Cuera slope. Panel shows correlation of slope deposits between red-stained intervals RL-A and RL-B. Note sequence boundary (sb) placed (sections 1 to 4) at the base of a boundstone or grainstone interval (lowstand deposits), which overlies breccia with upper-slope material (latest highstand deposits). In the lower slope the sb is interpreted at the base of a significant grainstone interval with platform-derived material interpreted as lowstand or early transgressive deposits. Red-stained lenticular bodies present in the upper slope, deposited during early transgression or early highstand, are likely to be the result of minor sea-level oscillations.

microfractures, in contrast to radial fibrous calcite, which is inclusion rich. Under CL, this phase is largely nonluminescent, with individual crusts being separated by a thin layer of bright-luminescent calcite (Fig. 8B).

Diagenetic Environment.—Following previous work (e.g., Kaufmann 1997 and references therein), the change in crystal morphology, inclusion density, and cathodoluminescence characteristics between fibrous and syntaxial, scalenohedral overgrowth calcite cement is interpreted as the result of a change in fluid composition related to a change in diagenetic environment. A widely accepted interpretation for this change in cement

type is the transition from the marine to the meteoric (Carpenter and Lohmann 1989; Csoma et al. 2004) or from the marine to the shallow-burial domain (Zeeh et al. 1995). There is no field, geochemical, or petrographic evidence for subaerial exposure such as the presence of a corrosion surface between the rfc and overgrowth cement or a break in cementation. The overgrowth cements that rim radiaxial fibrous calcite precipitated in several hundreds of meters of paleo-water depth. A meteoric origin for this change in cement facies is thus unlikely and is not supported by any kind of direct or circumstantial evidence. From this it concludes that the transition from fibrous to scalenohedral overgrowth cement reflects the change from marine to shallow-burial diagenesis.

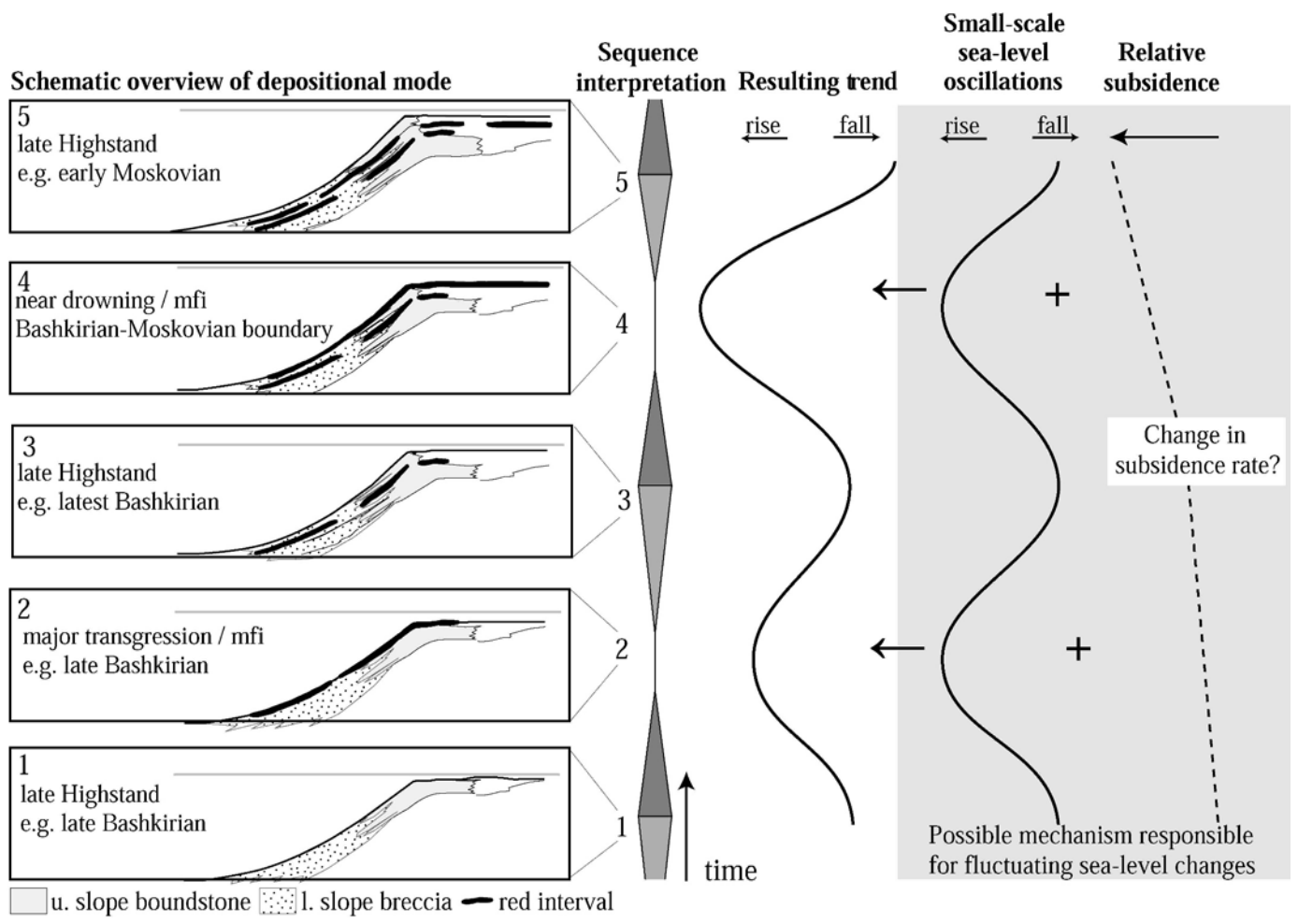


FIG. 11.—Depositional model of red-stained interval in a sequence stratigraphic context. The red intervals are deposited during transgressive pulses. Mechanisms suggested include the combined effect of glacio-eustasy and a change in relative subsidence.

Carbon and Oxygen Isotope Trends

Observations.—The carbon-isotope composition of matrix micrite and radial fibrous calcite from red intervals is consistent throughout slope transects and within stratigraphic sections (Fig. 13). In contrast, $\delta^{13}\text{C}$ ratios of brachiopod shells have a wider range. The $\delta^{13}\text{C}$ ratios of the different carbonate materials range between 4.8 and 5.8‰ for matrix samples, between 5.1 and 5.7‰ for fibrous calcites, and between 4.7 and 6.1‰ for brachiopods (Fig. 13A).

The $\delta^{18}\text{O}$ values of matrix micrites and radial fibrous cements are more variable than carbon isotopes. Matrix micrite and fibrous cement $\delta^{18}\text{O}$ ratios from red intervals range from about -3 to 1 ‰. In contrast, $\delta^{18}\text{O}$ values of red-interval brachiopods define a much narrower field of -2 to 0.5 ‰. Fibrous-cement $\delta^{18}\text{O}$ ratios are between -4 and 0.5 ‰ (Fig. 13A). Oxygen-isotope values from gray boundstone micrites and

fibrous cements range from -8 to -1 ‰ (matrix) and -7 to -1 ‰ (rfc; Fig. 13A).

Oxygen-isotope data of matrix micrites, fibrous cements, and brachiopods collected from red intervals do not match (Fig. 13A). Matrix micrite $\delta^{18}\text{O}$ values are on average as much as 1 to 2 ‰ higher than brachiopod $\delta^{18}\text{O}$ ratios and < 1 to 2 ‰ higher than fibrous calcites. This observation is uncommon, in that micritic carbonate is in many cases most affected by diagenetic alteration and hence display lower $\delta^{18}\text{O}$ ratios. Figure 13B summarizes $\delta^{13}\text{C}$ and $\delta^{18}\text{O}$ values of a single hand specimen documenting the internal geochemical variability of samples, and providing estimates for error bars that must be attached to these data sets.

Interpretation.—Two non-environmental factors could explain the wider range in brachiopod $\delta^{13}\text{C}$ relative to matrix micrite and radial

TABLE 3A.—Carbon-isotope composition of matrix micrites, marine cements, and brachiopod shells.

$\delta^{13}\text{C}$	Red-interval matrix micrite	Gray-interval matrix micrite	Red-interval rfc	Gray-interval rfc	Red-interval brachiopod shell
Mean value	5.4‰	5.3‰	5.3‰	5.2‰	5.4‰
Standard deviation (σ)	0.3	0.3	0.3	0.2	0.6
Population (n)	131	310	41	75	25

TABLE 3B.—Oxygen-isotope composition of matrix micrites, marine cements, and brachiopod shells.

$\delta^{18}\text{O}$	Red-interval matrix micrite	Gray-interval matrix micrite	Red-interval rfc	Gray-interval rfc	Red-interval brachiopod shell
Mean value	−0.7‰	−3.8‰	−1.8‰	−4.2‰	−1.7‰ to 0.5‰
Standard deviation (σ)	1.5	2.0	2.2	2.7	0.6
Population (n)	131	310	41	75	25

fibrous calcite: firstly, vital or metabolic effects and the sampling location within a specific shell (i.e., primary, secondary, and tertiary shell, cardinal process, pedicle foramen; Parkinson et al. 2005). Depending on the sampling locality, values can scatter by as much as 2‰ within a single shell. Secondly, it is possible that both matrix micrites and fibrous cements displayed a similarly wide or even wider range in carbon-isotope ratios during initial deposition, reflecting open-seawater chemistry. If this is the case, early marine diagenetic porewater alteration and isotopic resetting might have equilibrated and reduced this inherited scatter to a narrower range. In contrast, the more stable low-Mg brachiopod calcite preserved their initial isotopic composition (including the wider data range).

The wide range of $\delta^{18}\text{O}$ data observed in matrix micrite and radialial fibrous calcite (Fig. 13) is best explained by variable degrees of diagenetic overprint. In the case of radialial fibrous calcite, some samples have Mn concentrations of > 400 ppm (Fig. 13C), indicative of nonmarine fluids (Bruckschen et al. 1999). Various degrees of diagenetic alteration of radialial fibrous calcites and carbonate matrix are recognized under CL. Irregular patches of brightly luminescent calcite cement locally replace fibrous cements (Fig. 8B), and in some places thin veins crosscut the matrix micrite.

Source of Iron in Red Intervals

Red intervals are characterized by increased concentrations of clay particles and iron in red-interval matrix micrite with respect to the overlying and underlying boundstone (Table 3). This could suggest an increased argillaceous influx from either the continent or by basin-parallel transport of suspended material via geostrophic currents. A strong influence of the nearby continent and possibly a detrital origin of iron in seawater are supported by the epeiric setting of the Sierra de Cuera platform (Fig. 2E). Alternatively, the argillaceous basinal sediments that interfinger with the toe-of-slope facies (RL7) might present a source of iron and clay particles. An increase in the clay-carbonate ratio associated with red-interval deposition might simply be the consequence of an overall decreased carbonate sedimentation rate (whilst clay depositional rates remained constant).

DISCUSSION

Origin of Red Staining

Diagenetic Environment.—Three observations suggest a synsedimentary or early diagenetic origin of reddening of the red intervals in the Sierra del

Cuera. First, pigmentation and different pigmentation intensities follow sedimentological features such as bioturbation and geopetals (Fig. 7, 8). Second, pores in crinoid ossicle pores are filled with red sediment and subsequently became occluded by syntaxial early marine cements. Third, late diagenetic iron remobilization and precipitation occurs only in stylolites and dissolution seams forming pyrite (Fig. 8). These observations are consistent with previous work (Mamet and Preat 2006, and references therein).

Iron Oxidation.—Iron oxidation of surface sediments is driven by abiotic and biotic processes. These mechanisms include slow sedimentation in an oxic environment as described in Boulvain et al. (2001), a change from anoxic to oxic sea water (Hu et al. 2005), or a change in depositional framework (Bourque and Boulvain 1993). In the case of the Sierra del Cuera red intervals, abiotic oxidation processes seem unlikely. Abiotic oxidation of iron in the red intervals resulting from low sedimentation rates cannot explain the observed pigmentation patterns, i.e., the small-scale distribution of iron pigment linked to specific facies types, sedimentological patterns, and skeletal fragments (Fig. 8). A change from anoxic to oxic depositional conditions is similarly unlikely. Anoxia or, more specifically, a change from anoxic to oxic water masses during boundstone or red-interval deposition is not supported by any field, petrographic, or geochemical evidence.

Iron oxidation involving iron bacteria (Bourque and Boulvain 1993; Preat et al. 2006, and references therein) is supported by several petrographic observations: foraminifer-chamber, bryozoan-zooecia, and microboring infill sediment (Fig. 8) are iron-stained. Furthermore, a relationship between red staining and tectonic features (Mamet and Preat 2006) is absent. Most significantly, molds of iron bacteria filaments (Fig. 8; cf. Mamet et al. 1997) are present. Geochemical evidence suggested by Boulvain et al. (2001) and Preat et al. (2006) of low Fe concentrations (< 350 ppm) in their examples of Phanerozoic red carbonates is not consistent with the elevated iron concentrations measured in the matrix micrites of the red intervals (Table 3). Iron availability does not appear to be a limiting factor for iron bacteria (Kappler and Newman 2003).

Red staining of Sierra de Cuera slope intervals thus likely took place under the influence of iron-oxidizing bacteria. This implies the presence of low-oxygen water masses (Mamet and Preat 2006), which is not consistent with the interpretation of oxygen-rich and cold upwelling waters. Iron likely oxidized within the pore water contained in the sediment pile near but not at the sediment surface. Within the pore water, oxygen is rapidly consumed by the oxidation of organic matter.

TABLE 3C.—Trace-element concentrations in marine cements and matrix micrites.

Trace elements	Mg (ppm)	Fe (ppm)	Sr (ppm)	Mn (ppm)	population
Marine cements average (range)	5852 (4202–7159)	169 (bdl* ¹ –233)	341 (253–469)	344 (91–719)	22
Red-matrix micrite average (range)	5675 (3588–7943)	641 (395–991)	174 (147–182)	(bdl–244)	10
Gray-automicrite average (range)	3211 (1855–5453)	177 (83–428)	203 (160–317)	(bdl–164)	10

*¹) bdl = below detection limit

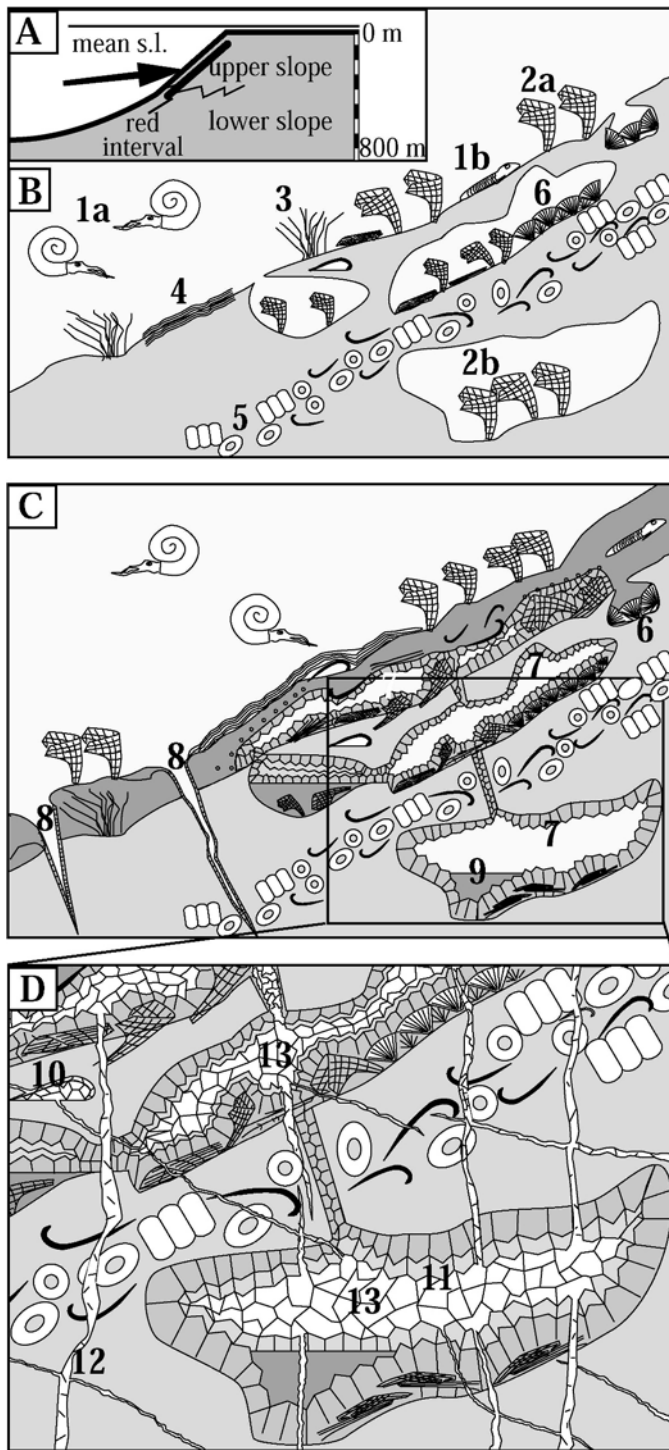


FIG. 12.—Schematic diagram of marine and shallow-burial diagenetic events. A) Schematic overview of Sierra del Cuera carbonate platform. Arrow indicates location of schematic diagram of diagenetic events. B) Initial setting: ammonoids (1a), trilobites (1b), fenestellid bryozoans at the seafloor (2a) and in cavities (2b), algae (3), algal mats (4), interbedded brachiopod-rich and crinoid-rich layers (5). C) Marine diagenetic features: botryoidal cement (6) and isopachous rims of radial fibrous calcite (7), syndimentary fractures (8), and internal sediment (9). D) Early-burial diagenetic features include dissolution of unstable shell material (10), scalenohedral overgrowth cement (11), fractures (12), and equant mosaic calcite cement (13).

Origin of Biocementstone

One of the most intriguing aspects of the Sierra del Cuera red intervals is the volumetrically significant biocementstone: facies RL2, 3, 5 (Fig. 4). Cementstones are common in Paleozoic mounds (James and Gravestock 1990; Webb 1996; Boulvain 2001) and less so in the Mesozoic (Neuweiler et al. 2001; Aubrecht et al. 2002; Aubrecht and Szulc 2006; Neuweiler and Bernoulli 2005a, 2005b). Reasons for this might include a change in seawater geochemistry and/or differing platform ecosystems (Neuweiler et al. 2001). Furthermore, cementstones RL2 and RL3 are associated with firmgrounds. Carboniferous bryozoans (Taylor and Wilson 2003) and the brachiopods present on the Sierra del Cuera (Martinez-Chacon and Bahamonde 2005) typically grew on biotic or cryptic hard substrates and firmgrounds, or paleo-cavities.

Following previous work of Walls and Burrowes (1985), Kerans et al. (1986), Horbury (1992), Gischler (1995), and Webb (1996), high cementation rates are considered one of the main factors for the formation of cementstone and the stabilization of red-stained intervals, whilst evidence for (microbial) automicrite within these intervals is lacking. High cementation rates are indicated by: firstly, the cementation of *in situ* or minor reworked fenestellid bryozoans (Fig. 7, 8) and brachiopods, and secondly, the abundance of marine cement with respect to an overall lack of internal sediment. The detailed assessment of the mechanisms that drove extensive cementation at greater water depths is the topic of a companion paper.

In conclusion, low sedimentation rates and high cementation rates, the presence of scaffold constructors, firmgrounds or hardgrounds, and specific chemical and physical oceanographic conditions during red-interval deposition all support the formation of biocementstone.

Paleoceanographic Implications of Red Intervals

During the Pennsylvanian, the Cantabrian Arc (now Cantabrian zone, Fig. 2B) and the Sierra del Cuera platform were located between 10 and 20° south, in an epicritic foreland setting (Fig. 2). Red intervals formed during transgressive events (Fig. 11; Bahamonde et al. 2004; Kenter et al. 2005) in a depositional environment below the photic zone and below the effective wave base. Immenhauser et al. (2002) suggested that during pronounced transgressive events (i.e., red-interval deposition) cool basinal waters were lifted onto—and hence flooded—the platform top. Inasmuch as this hypothesis is difficult to document for a fossil platform, the lines of evidence are circumstantial.

Cooler water masses during red-interval deposition are interpreted from a consistent increase of at least 2‰ in $\delta^{18}\text{O}$ of red-interval micrites and marine cements with respect to those of gray boundstone representing normal conditions (Fig. 13). It is accepted that matrix micrite and less so marine cements are prone to diagenetic alteration, but there is no petrographic and geochemical evidence to support facies-specific diagenesis (Immenhauser et al. 2002). Applying the temperature equations of Kim and O'Neil (1997) on the measured oxygen isotope data (assuming 0‰ V-SMOW), the average paleo-seawater temperature on the slope would be at least 12°C lower during red-interval deposition than during boundstone deposition.

Alternative interpretations explaining changes in the seawater $\delta^{18}\text{O}$ values on the platform top, including waxing and waning of continental ice and enhanced evaporation (Allan and Matthews 1982) seem unlikely. Meltwater-driven glacio-eustatic sea-level rise would suggest a $\delta^{18}\text{O}$ shift towards lower $\delta^{18}\text{O}$ values (Bickert 2000), i.e., the opposite of what is observed. Taking into account that a significant rise in sea level was one of the driving factors of red-interval sedimentation, the effect of enhanced evaporation rates on the deeply flooded platform top would be negligible. In contrast, geochemical evidence for cooler, deeper water is supported by the biota. In addition to a cool-water, heterozoan assemblage (*sensu* James 1997), a prominent light-independent facies (crinoid-rich pack-

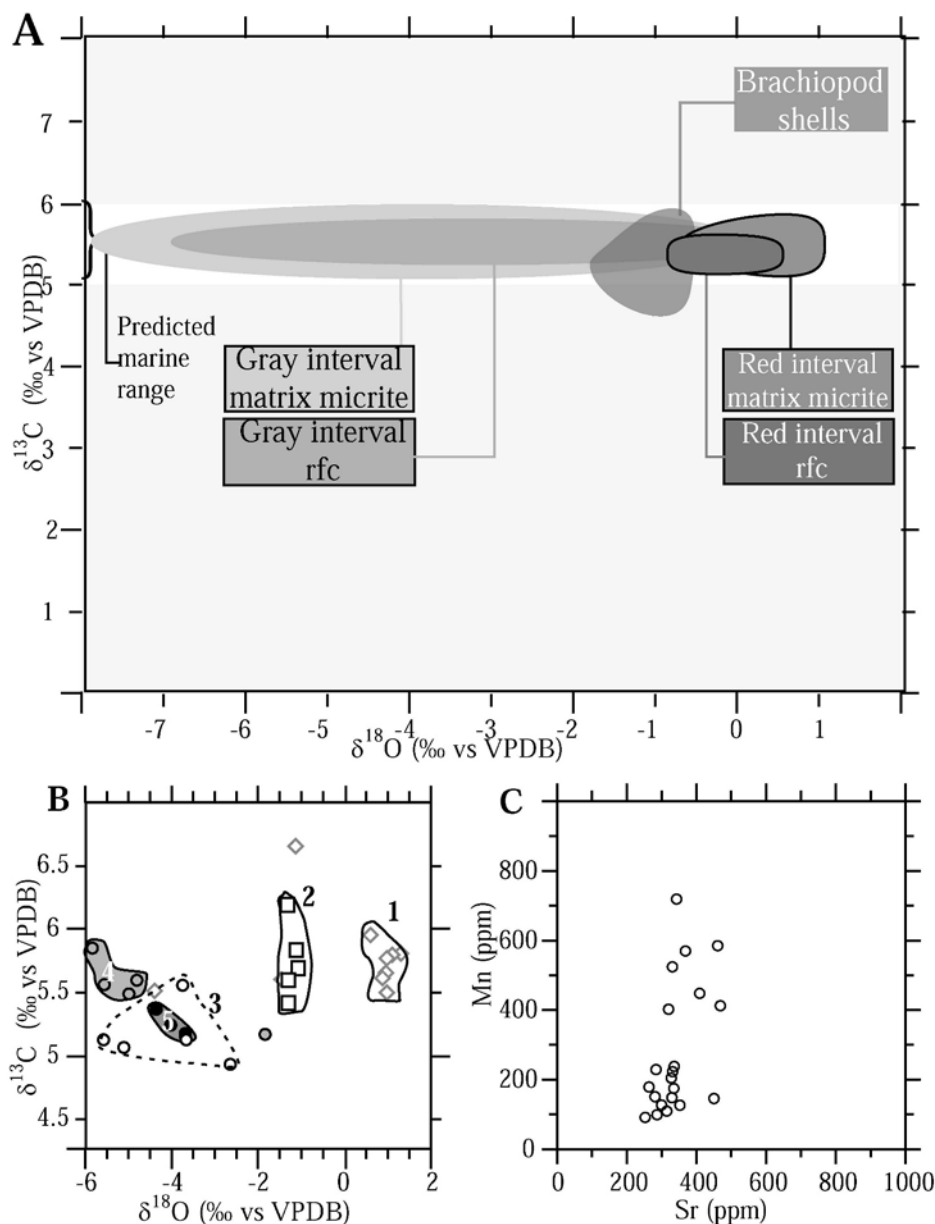


FIG. 13.—A) Carbon- and oxygen-isotope data of matrix micrite, rfc, and brachiopod shells from the Sierra del Cuera slope. The predicted marine $\delta^{13}\text{C}$ range is from Bruckschen et al. (1999). Note that $\delta^{18}\text{O}$ values of red-interval carbonates are higher than low-Mg brachiopod shells and those of gray carbonates. Areas bordered by dotted lines refer to deviating but still significant amount of red-interval matrix micrite and radiaxial calcite values. B) Carbon- and oxygen-isotope data of matrix micrite, rfc, and bulk brachiopods from a single red-interval hand specimen collected in the upper slope. 1 = matrix micrite, 2 = brachiopod shell, 3 = radiaxial calcite, 4 = scalenohedral overgrowth calcite, 5 = blocky calcite. Note geochemical trends similar to those in Figure A. C) Manganese and Sr concentrations in rfc.

stones, RL4) is present on the platform top during red-interval sedimentation.

A significant decrease in ambient seawater temperature could explain the absence of microbial boundstone during red-interval deposition. Microbially induced mineralization by, e.g., calcifying cyanobacteria (Della Porta 2003) favors elevated seawater temperature (Riding 1992). A significant decrease in seawater temperature might cause a halt to a microbially induced carbonate factory.

In addition to lower sea-water temperatures, nutrient gradients require consideration. The abundance of bryozoans, crinoids, and brachiopods during red-interval deposition on the Sierra del Cuera slope is in line with an elevated nutrient level in ambient seawater. Similar interpretations are known from modern reefs (Mutti and Hallock 2003; Vecsei 2003; Halfar et al. 2004; Halfar et al. 2006) and other fossil carbonate carbonate settings (Peterhaensel and Pratt 2001; Stemmerik 2001; Samankassou 2002; Ehrenberg et al. 2006). Hallock and Schlager (1986) showed that nutrient excess in modern tropical reefs could lead to the establishment of a heterozoan community.

Mesotrophic seawater levels are in contrast to the oligotrophic conditions required by the interpretation of iron bacteria (Mamet and Preat 2006). Based on observations presented here and on the diversity of paleo-environments from which red carbonates are reported (Table 1), it is concluded that iron bacteria probably thrive in a range of marine environments with variable nutrient contents and hydrodynamic conditions.

A driver for cooler water masses and elevated nutrient levels is upwelling. Mutti and Hallock (2003 and references therein), report mesotrophic to eutrophic conditions for modern equatorial and meridional upwelling zones respectively. Samankassou (2002) interpreted a change from a typical tropic biotic assemblage to a cool-water association similar to that of the Sierra del Cuera red intervals, by a change in seawater temperature, possibly linked with increased nutrient fluxes and coastal upwelling.

Coastal upwelling was also suggested by Immenhauser et al. (2003) as a possible mechanism to explain a 3.5‰ shift to higher $\delta^{18}\text{O}$ ratios on the Sierra del Cuera inner platform during red-interval deposition. Temper-

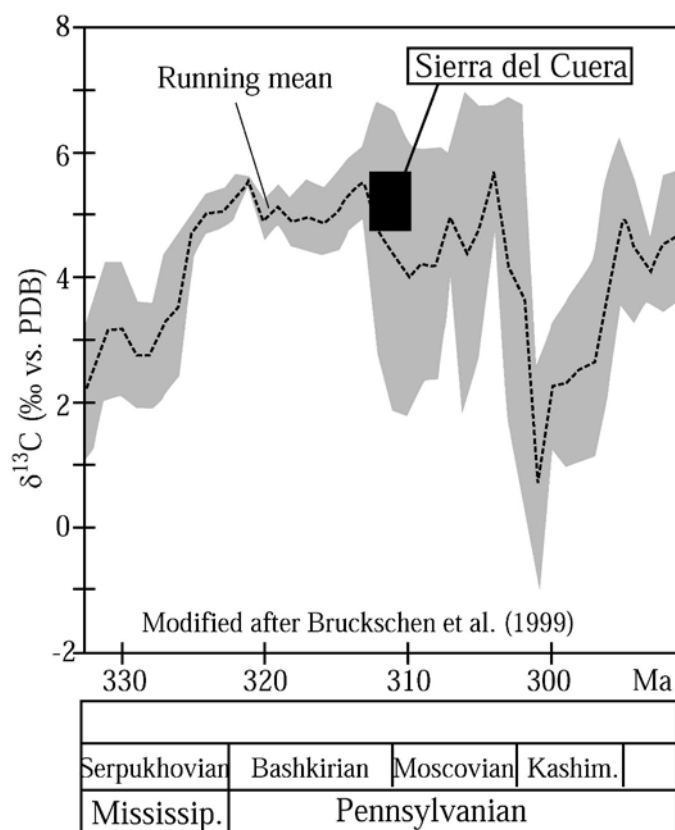


FIG. 14.—Carbon-isotope range of the Sierra del Cuera slope matrix micrite, rfc, and brachiopod shells plotted on the Pennsylvanian carbon-isotope curve for open marine seawater from Bruckschen et al. (1999).

ature alone seems an insufficient mechanism to explain this shift, inasmuch as it would imply a temperature drop in seawater on the platform top on the order of 15 to 16°C (Immenhauser et al. 2003). Although along the slope, the $\delta^{18}\text{O}$ shift appears, on average, less pronounced (2–3‰, e.g., 12–15°C) compared to the platform top, $\delta^{18}\text{O}$ shifts from gray boundstone to red intervals are in several cases on the order of 3–4‰ (Immenhauser et al. 2002), similar to the platform top.

The effect of upwelling on the carbon-isotope composition in carbonate rocks is uncertain. Surface water, normally enriched in ^{13}C (Bickert 2000), becomes relatively depleted during upwelling. However, productivity increases with upwelling, causing higher $\delta^{13}\text{C}$. The combined effect of these factors on the $\delta^{13}\text{C}$ in the carbonate sediments is uncertain. The consistent pattern observed in the $\delta^{13}\text{C}$ (Fig. 13) might well be the result of the combined effect of upwelling and productivity.

In conclusion, the most likely drivers of basal water flooding of the platform top include an elevated (seasonal) thermocline due to maximum sea level, as well as upwelling of cooler basal water as observed in many modern marginal seas such as in the Arabian Gulf (Shi et al. 2000).

Implications for Paleobathymetric Estimates in Carboniferous Outer-Platform and Peri-Platform Sedimentary Rocks

An obvious strength of this study is the quantitative bathymetric control on the red-interval facies distribution in the Sierra del Cuera. Assuming a glacioeustatic sea-level change on the order of 40 meters (Maynard and Leeder 1992) and sediment buildup during transgressive intervals of 8 meters and less (crinoidal bars; Della Porta et al. 2004), the depth of the early Moscovian platform break during red-interval

deposition was approximately 32–40 meters. Although this is a coarse approximation only, the estimation aids in assessing slope paleo-water depths. Using the paleo-bathymetric framework from the Sierra del Cuera, water-depth ranges can be assigned tentatively to other similar Carboniferous facies where bathymetric control is lacking.

The presence of red carbonates depends on local physical and chemical oceanographic, biotic, and sedimentological factors, physiographic setting, and antecedent topography. Therefore not all red carbonates, such as the Ammonitico Rosso (Jenkyns 1974) or Cretaceous oceanic red beds (Hu et al. 2005), are comparable with the Sierra del Cuera red-interval facies (Fig. 1). Within these limitations, specific red-interval facies types of the Sierra del Cuera slope can be linked to specific depth intervals whereas other facies types are depth independent (Fig. 5). Three depth-dependent and a depth independent categories are distinguished.

(1) *Inner platform and upper slope*: Skeletal wackestone and packstone facies (RL1; Fig. 5) is present both on the inner platform and upper slope. The depth range is from at least 30–40 (Maynard and Leeder 1992) to approximately 400 meters. The Middle Jurassic Oolithe ferrugineuse de Bayeux Formation (France) includes facies types similar to the RL1 red-interval facies in the Sierra del Cuera. Preat et al. (2000) proposed a depositional water depth of at least 100 meters. The Sierra del Cuera study adds solid and direct evidence to this estimate. The absence of volumetrically important volumes of marine cements in the Oolithe ferrugineuse de Bayeux Formation is similar to especially the protected inner platform or the mid-slope setting of RL1. The Middle Jurassic Brocatello and Besazio limestones (Neuweiler and Bernoulli 2005a) were deposited in a deeper marine depositional environment with a minimum water depth of 50 meters. Again this assessment is supported by direct bathymetric evidence from this study (RL1).

(2) *Upper slope*: Brachiopod, bryozoan, and biocementstone facies (RL2, RL3, RL5; Fig. 5) are estimated to have accumulated in water depths of 40 to 250 meters on the Sierra del Cuera. To our knowledge, examples of red carbonates characterized by biocementstones have not been reported in the literature.

(3) *Upper and lower slope*: Red-matrix breccia and toe-of-slope red mudstone redeposited facies (RL6, RL7; Fig. 5) are present from several hundreds of meters of water depth to the lower slope. This implies that the depositional depth window is determined largely by the antecedent topography, i.e., the slope angle and the overall relief of the carbonate buildup and platform slope.

(4) *Depth-independent facies*: Red-stained crinoid packstones and rudstones (RL4; Fig. 5) are present in the outer platform in paleo-water depths of approximately 40 meters (Maynard and Leeder 1992). The same facies was also shed onto the upper and lower slope, i.e., down to water depths of over 600 meters. This implies that no specific bathymetric significance should be attributed to this facies.

CONCLUSIONS

(1) Seven red intervals (each 5–30 meters thick) are recognized in the platform top and slope of the Bashkirian–Moscovian Sierra del Cuera carbonate platform in northern Spain. On the upper slope (0–350 m below platform break), red intervals alternate with microbial and algal boundstone. On the lower slope (350–700 m below platform break), red-matrix breccias form tabular or lenticular bodies in clast-supported breccia facies.

(2) Within these red intervals, seven lithofacies types were identified. Five of these can be attributed to a specific range in depositional depth, including the inner platform and upper slope (30–40 to approximately 400 m water depth) and the upper and lower slope (several hundreds of meters to approximately 800 m). In the case of cementstones the bathymetric occurrence is probably linked to specific and favorable physical and chemical seawater conditions.

(3) From the viewpoint of transgressive–regressive cycles and sequence stratigraphy, red intervals record maximum flooding intervals. Consequently, each red interval on the slope, and its lateral counterpart in the outer platform, registers a major transgressive event. Only two red intervals extending into the inner platform are preserved, which record episodes of near-platform drowning. The driving factor of rapid sea-level rise is likely glacio-eustasy (eccentricity-driven) in addition to a change (increase) in tectonic subsidence.

(4) Red staining of these intervals was probably an early diagenetic process, involving iron-oxidizing bacteria—an interpretation consistent with previous studies. The source of iron is tentatively assigned to continental influx. The staining took place within the upper decimeters to meters of the sediment column, probably driven by suboxic pore-waters.

(5) Upwelling of cold, nutrient-rich basinal seawater onto the upper slope; and cool water masses across the platform cause increasing eutrophication. These conditions favored the transient establishment of heterozoan biotic associations that characterize the red intervals.

(6) This study and particularly the combination of sedimentological, paleo-ecological, bathymetric, and geochemical evidence are of use for the interpretation of Paleozoic red-stained intervals in other basins and platforms lacking a bathymetric control.

ACKNOWLEDGMENTS

We acknowledge M.L. Martínez Chacón for identification of the brachiopod specimens. W. Schlager, G. Della Porta, and J. Kenter are thanked for making data available and for constructive comments, and A. Csoma for help with the interpretation of carbonate diagenetic phases. N. Koort, B. Lacet, and F. Bakker produced high-quality thin sections and slabs, and S. Verdegaal, H. Vonhof, K. Slimmen, and K. Beets supported us in the stable-isotope and trace-element laboratory of the Vrije Universiteit. Critical comments and suggestions by editor K. Milliken, associate editor M. Elrick, and reviewers G. Soreghan, S. Egenhoff, and P. Holterhoff are acknowledged.

REFERENCES

ALLAN, J.R., AND MATTHEWS, R.K., 1982, Isotope signatures associated with early meteoric diagenesis: *Sedimentology*, v. 29, p. 797–817.

AUBRECHT, R., AND SZULC, J., 2006, Deciphering of the complex depositional and diagenetic history of a scarp limestone breccia (Middle Jurassic Krasin Breccia, Pieniny Klippen Belt, Western Carpathians): *Sedimentary Geology*, v. 186, p. 265–281.

AUBRECHT, R., SZULC, J., MICHALIK, J., SCHLOGL, J., AND WAGREICH, M., 2002, Middle Jurassic stromatolite mud-mound in the Pieniny Klippen Belt (Western Carpathians): *Facies*, v. 47, p. 113–126.

BAHAMONDE, J.R., COLMENERO, J.R., AND VERA, C., 1997, Growth and demise of late Carboniferous carbonate platforms in the eastern Cantabrian Zone, Asturias, northwestern Spain: *Sedimentary Geology*, v. 110, p. 99–122.

BAHAMONDE, J.R., KENTER, J.A.M., DELLA PORTA, G., KEIM, L., IMMENHAUSER, A., AND REIJMER, J.J.G., 2004, Lithofacies and depositional processes on a high, steep-margined Carboniferous (Bashkirian–Moscovian) carbonate platform slope, Sierra del Cuera, NW Spain: *Sedimentary Geology*, v. 166, p. 145–156.

BAHAMONDE, J.R., MERINO-TOMÉ, O., AND HEREDIA, N., 2007, A Pennsylvanian microbial boundstone-dominated carbonate shelf in a distal foreland margin (Picos de Europa Province, NW Spain): *Sedimentary Geology*, v. 3–4, p. 167–193.

BATHURST, R.G.C., 1977, Ordovician Meiklejohn bioherms, Nevada: *Geological Magazine*, v. 114, p. 308–311.

BICKERT, T., 2000, Influence of geochemical processes on stable isotope distribution in marine sediments, in Schulz, H.D., and Zabel, M., eds., *Marine Geochemistry*: Heidelberg, Springer-Verlag, p. 309–334.

BOULVAIN, F., 2001, Facies Architecture and diagenesis of Belgian late Frasnian carbonate mounds: *Sedimentary Geology*, v. 145, p. 269–294.

BOULVAIN, F., DE RIDDER, C., MAMET, B., PREAT, A., AND GILLAN, D., 2001, Iron microbial communities in Belgian Frasnian carbonate mounds: *Facies*, v. 44, p. 47–59.

BOURQUE, P.-A., AND BOULVAIN, F., 1993, A model for the origin and petrogenesis of the red stromatolite limestone of Paleozoic carbonate mounds: *Journal of Sedimentary Petrology*, v. 63, p. 607–619.

BRUCKSCHEN, P., OESMANN, S., AND VEIZER, J., 1999, Isotope stratigraphy of the European Carboniferous: proxy signals for ocean chemistry, climate and tectonics: *Chemical Geology*, v. 161, p. 127–163.

CARPENTER, S.J., AND LOHMANN, K.C., 1989, $\delta^{18}\text{O}$ and $\delta^{13}\text{C}$ variations in Late Devonian marine cements from the Golden Spike and Nevis reefs, Alberta, Canada: *Journal of Sedimentary Petrology*, v. 59, p. 792–814.

CLARKSON, E.N.K., 1996, *Invertebrate Paleontology and Evolution*: London, Chapman & Hall, 434 p.

COLMENERO, J.R., AGUEDA, J.A., BAHAMONDE, J.R., BARBA, F.J., BARBA, P., FERNANDEZ, L.P., AND SAMLVADOR, C.I., 1993, Evolución de la cuenca de antepais Namuriense y Westfaliense de la Zona Cantábrica, NW de España: XII International Congress Carboniferous–Permian, Buenos Aires, *Comptes Rendus*, v. 2, p. 175–190.

CSOMA, A.E., GOLDSTEIN, R.W., MINDSZESTY, A., AND SIMONE, L., 2004, Diagenetic salinity cycles and sea level along a major unconformity, Monte Camposauro, Italy: *Journal of Sedimentary Research*, v. 74, p. 889–903.

DELLA PORTA, G., 2003, Depositional anatomy of a Carboniferous high-rising carbonate platform (Cantabrian Mountains, NW Spain) [Unpublished Ph.D. Thesis]: Vrije Universiteit Amsterdam, 250 p.

DELLA PORTA, G., KENTER, J.A.M., IMMENHAUSER, A., AND BAHAMONDE, J.R., 2002, Lithofacies character and architecture across a Pennsylvanian inner-platform transect (Sierra de Cuera, Asturias, Spain): *Journal of Sedimentary Research*, v. 72, p. 898–916.

DELLA PORTA, G., KENTER, J.A.M., BAHAMONDE, J.R., IMMENHAUSER, A., AND VILLA, E., 2003, Microbial boundstone dominated carbonate slope (Upper Carboniferous, N Spain): microfacies, lithofacies distribution and stratal geometry: *Facies*, v. 49, p. 175–208.

DELLA PORTA, G., KENTER, J.A.M., AND BAHAMONDE, J.R., 2004, Depositional facies and stratal geometry of an Upper Carboniferous prograding and aggrading high-relief carbonate platform (Cantabrian Mountains, N Spain): *Sedimentology*, v. 51, p. 267–295.

DETTMAN, D.L., AND LOHMANN, K.C., 1995, Microsampling carbonates for stable isotope and minor element analysis: physical separation on a 20 micrometer scale: *Journal of Sedimentary Research*, v. 65, p. 566–569.

DONAGHAY, P.L., 1991, The role of episodic atmosphere nutrient inputs in chemical and biological dynamics of oceanic ecosystems: *Oceanography*, v. 4, p. 62–70.

EHRNBERG, S.N., MCARTHUR, J.M., AND THIRLWALL, M.F., 2006, Growth, demise, and dolomitization of Miocene carbonate platforms on the Marion Plateau, offshore NE Australia: *Journal of Sedimentary Research*, v. 76, p. 91–116.

ELRICK, M., AND READ, J.F., 1991, Cyclic ramp-to-basin carbonate deposits, lower Mississippi, Wyoming, and Montana—a combined field and computer modeling study: *Journal of Sedimentary Petrology*, v. 61, p. 1194–1224.

GISCHLER, E., 1995, Current and wind-induced facies patterns in a Devonian atoll—Iberg Reef, Harz Mts, Germany: *Palaos*, v. 10, p. 180–189.

GRADSTEIN, F., AND OGG, J.G., 2004, Geological timescale for the Phanerozoic: *Episodes*, v. 19, p. 3–4.

HAASE, R.R., 2000, The reactivation of iron, in Schulz, H.D., and Zabel, M., eds., *Marine Geochemistry*: Heidelberg, Springer-Verlag, p. 233–262.

HALFAR, J., GODINEZ-ORTA, L., MUTTI, M., VALDEZ-HOLGUIN, J.E., AND BORGES, J.M., 2004, Nutrient and temperature controls on modern carbonate production: an example from the Gulf of California, Mexico: *Geology*, v. 32, p. 213–216.

HALFAR, J., GODINEZ-ORTA, L., MUTTI, M., VALDINEZ-HOLGUIN, J.E., AND BORGES, J.M., 2006, Carbonates calibrated against oceanographic parameters along a latitudinal transect in the Gulf of California, Mexico: *Sedimentology*, v. 53, p. 297–320.

HALLOCK, P., AND SCHLAGER, W., 1986, Nutrient excess and the demise of coral reefs and carbonate platforms: *Palaos*, v. 1, p. 389–398.

HECKEL, P.H., 1986, Sea-level curve for the Pennsylvanian eustatic marine transgressive–regressive depositional cycles along midcontinent outcrop belt, North America: *Geology*, v. 14, p. 330–334.

HECKEL, P.H., 1994, Evaluation of evidence for glacio-eustatic control over marine Pennsylvanian cyclothem in North America and consideration of possible tectonic effects: *SEPM, Concepts in Sedimentology and Paleontology*, n. 4, p. 65–87.

HORBURY, A.D., 1992, A Late Dinantian peloid cementstone–palaecoberesellid buildup from North Lancashire, England: *Sedimentary Geology*, v. 79, p. 117–137.

HU, X.M., JANSZ, L., WANG, C.S., SARTI, M., BAK, K., WAGREICH, M., MICHALIK, J., AND SOTAK, J., 2005, Upper Cretaceous oceanic red beds (CORBs) in the Tethys: occurrences, lithofacies, age, and environments: *Cretaceous Research*, v. 26, p. 3–20.

IMMENHAUSER, A., KENTER, J.A.M., GANSEN, G., BAHAMONDE, J.R., VAN VLIET, A., AND SAHER, M.H., 2002, Origin and significance of isotope shifts in Pennsylvanian carbonates (Asturias, NW Spain): *Journal of Sedimentary Research*, v. 72, p. 82–94.

IMMENHAUSER, A., DELLA PORTA, G., KENTER, J.A.M., AND BAHAMONDE, J.R., 2003, An alternative model for positive shifts in shallow marine carbonate $\delta^{13}\text{C}$ and $\delta^{18}\text{O}$: *Sedimentology*, v. 50, p. 953–959.

JAMES, N.P., 1997, The cool-water carbonate depositional realms, in James, N.P., and Clarke, J.A.D., eds., *Cool-Water Carbonates, SEPM, Special Publication* 56, p. 1–20.

JAMES, N.P., AND GRAVESTOCK, D.I., 1990, Lower Cambrian shelf and shelf margin buildups, Flinders Ranges, South Australia: *Sedimentology*, v. 37, p. 455–480.

JENKYN, H.C., 1974, Origin of red nodular limestones (Ammonitico Rosso, Knollenkalke) in the Mediterranean Jurassic: a diagenetic model, in Hsu, K.J., and Jenkyn, H.C., eds., *Pelagic Sediments: on Land and Under the Sea*: Oxford, International Association of Sedimentologists, Special Publication 1, p. 249–272.

JENKYN, H.C., 1986, Pelagic environments, in Reading, H.G., ed., *Sedimentary Environments and Facies*: Oxford, U.K., Blackwell Scientific Publications, p. 314–371.

JULIVERT, M., 1971, Decollement tectonics in the Hercynian cordillera of northwest Spain: *American Journal of Science*, v. 270, p. 1–29.

- KAPPLER, A., AND NEWMAN, D.K., 2003, Formation of Fe(III)-minerals by Fe(II)-oxidizing photoautotrophic bacteria: *Geochimica and Cosmochimica Acta*, v. 68, p. 1217–1226.
- KAUFMANN, B., 1997, Diagenesis of Middle Devonian carbonate mounds of the Mader Basin (eastern Anti-Atlas, Morocco): *Journal of Sedimentary Research*, v. 67, p. 945–956.
- KENDALL, A.C., 1985, Radial fibrous calcite: a reappraisal, in Schneidermann, N., and Harris, P.M., eds., *Carbonate Cements*, SEPM, Special Publication 36, p. 59–77.
- KENTER, J.A.M., 1990, Carbonate platform flanks—slope angle and sediment fabric: *Sedimentology*, v. 37, p. 777–794.
- KENTER, J.A.M., HOEFLAKEN, F., BAHAMONDE, J.R., BRACCO-GARTNER, G.L., KEIM, L., AND BESEMS, R.E., 2003, Anatomy and lithofacies of an intact and seismic-scale Carboniferous carbonate platform (Asturias, NW Spain): analogues of hydrocarbon reservoirs in the Pricaspian Basin (Kazakhstan), in Zempolich, W.G., and Cook, H.E., eds., *Paleozoic Carbonates of the Commonwealth of Independent States (CIS): Subsurface Reservoirs and Outcrop Analogs*, SEPM, Special Publication 74, p. 185–207.
- KENTER, J.A.M., HARRIS, P.M., AND DELLA PORTA, G., 2005, Steep microbial boundstone-dominated platform margins—examples and implications: *Sedimentary Geology*, v. 178, p. 5–30.
- KERANS, C., HURLEY, N.F., AND PLAYFORD, P.E., 1986, Marine diagenesis in Devonian reef complexes of the Canning Basin, Western Australia, in Schroeder, J.H., and Purser, B.H., eds., *Reef Diagenesis*: New York, Springer-Verlag, p. 357–380.
- KIM, S.-T., AND O'NEIL, J.R., 1997, Equilibrium and non-equilibrium oxygen isotope effects in synthetic carbonates: *Geochimica and Cosmochimica Acta*, v. 61, p. 3461–3475.
- LEES, A., AND MILLER, J., 1995, Waulsortian banks, in Monty, C.L.V., Bosence, D.W.J., Bridges, P.H., and Pratt, B.R., eds., *Carbonate Mud-Mounds*: Oxford, U.K., Blackwell Science, p. 191–271.
- MAMET, B., AND PREAT, A., 2006, Iron-bacterial mediation in Phanerozoic red limestones: State of the art: *Sedimentary Geology*, v. 185, p. 147–157.
- MAMET, B., PREAT, A., AND DE RIDDER, C., 1997, Bacterial origin of the red pigmentation in the Devonian Slivenec Limestone, Czech Republic: *Facies*, v. 36, p. 173–187.
- MARTINEZ CHACÓN, M.L., AND BAHAMONDE, J.R., 2005, Brachiopods in the steep slope of a Pennsylvanian carbonate platform (Sierra del Cuera, Asturias, N. Spain): Fifth International Brachiopod Congress, University of Copenhagen: Denmark.
- MAYNARD, J.R., AND LEEDER, M.R., 1992, On the periodicity and magnitude of Late Carboniferous glacioeustatic sea-level changes: *Geological Society of London, Journal*, v. 149, p. 303–311.
- MENNING, M., ALEKSEEV, A.S., CHUVASHOV, B.L., DAVYDOV, V.I., DEVUYST, F.-X., FORKE, H.C., GRUNT, T.A., HANCE, L., HECKEL, P.H., IZOKH, N.G., JIN, Y.-G., JONES, P.J., KOTLYAR, G.V., KOZUR, H.W., NEMOYROVSKA, T.I., SCHNEIDER, J.W., WANG, X.-D., WEDDIGE, K., WEYER, D., AND WORK, D.M., 2006, Global time scale and regional stratigraphic reference scales of Central and West Europe, East Europe, Tethys, South China, and North America as used in the Devonian–Carboniferous–Permian Correlation Chart 2003 (DCP 2003): *Palaeogeography, Palaeoclimatology, Palaeoecology*, v. 240, p. 318–372.
- MII, H.-S., GROSSMAN, E.L., YANCEY, T.E., CHUVASHOV, B., AND EGOROV, A., 2001, Isotopic records of brachiopod shells from the Russian Platform—evidence for the onset of mid-Carboniferous glaciation: *Chemical Geology*, v. 175, p. 133–147.
- MUTTI, M., AND HALLOCK, P., 2003, Carbonate systems along nutrient and temperature gradients: some sedimentological and geochemical constraints: *International Journal of Earth Sciences (Geologische Rundschau)*, v. 92, p. 465–475.
- NEUWEILER, F., AND BERNOULLI, D., 2005a, Mesozoic (Lower Jurassic) red stromatactis limestones from the Southern Alps (Arzo, Switzerland): calcite mineral authigenesis and syneresis-type deformation: *International Journal of Earth Sciences*, v. 94, p. 130–146.
- NEUWEILER, F., AND BERNOULLI, D., 2005b, Erratum: Mesozoic (Lower Jurassic) red stromatactis limestones from the Southern Alps (Arzo, Switzerland): calcite mineral authigenesis and syneresis-type deformation: *International Journal of Earth Sciences*, v. 94, p. 130–146.
- NEUWEILER, F., BOURQUE, P.-A., AND BOULVAIN, F., 2001, Why is stromatactis so rare in Mesozoic carbonate mud mounds?: *Terra Nova*, v. 13, p. 338–346.
- PARKINSON, D., CURRY, G.B., CUSACK, M., AND FALICK, E., 2005, Shell structure, patterns and trends of oxygen and carbon stable isotopes in modern brachiopod shells: *Sedimentary Geology*, v. 219, p. 193–235.
- PETERHAENSEL, A., AND PRATT, B.R., 2001, Nutrient-triggered bioerosion and a giant carbonate platform masking the postextinction Famennian benthic community: *Geology*, v. 29, p. 1079–1082.
- PREAT, A., MAMET, B., BERNARD, A., AND GILLAN, D., 1999, Bacterial mediation, red matrices diagenesis, Devonian, Montagne Noire (southern France): *Sedimentary Geology*, v. 126, p. 223–242.
- PREAT, A., MAMET, B., DE RIDDER, C., BOULVAIN, F., AND GILLAN, D., 2000, Iron bacterial and fungal mats, Bajocian stratotype (Mid-Jurassic, northern Normandy, France): *Sedimentary Geology*, v. 137, p. 107–126.
- PREAT, A., MORANO, S., LOREAU, J.-P., AND DUREL, C., 2006, Petrography and biosedimentology of the Rosso Ammonitico Veronese (Middle–Upper Jurassic, north-eastern Italy): *Facies*, v. 52, p. 265–278.
- RIDING, R., 1992, Temporal variations in calcification in marine cyanobacteria: *Geological Society of London, Journal*, v. 149, p. 979–989.
- SAMANKASSOU, E., 2002, Cool-water carbonates in a paleoequatorial shallow-water environment: the paradox of the Auernig cyclic sediments (Upper Pennsylvanian, Carnic Alps, Austria–Italy) and its implications: *Geology*, v. 30, p. 655–658.
- SHI, W., MORRISON, J.M., BOHM, E., AND MANGHANANI, V., 2000, The Oman upwelling zone during 1993, 1994 and 1995: *Deep-Sea Research II*, v. 47, p. 1227–1247.
- STEMMERIK, L., 2001, Sequence stratigraphy of a low productivity carbonate platform succession: the Upper Permian Wegener Halvo Formation, Kastryggen Area, East Greenland: *Sedimentology*, v. 48, p. 79–97.
- STRASSER, A., HILGEN, F.J., AND HECKEL, P.H., in press, Cyclostratigraphy—concepts, definitions, and applications: *Newsletters on Stratigraphy*, v. 43.
- TAYLOR, P.D., AND WILSON, M.A., 2003, Paleocology and evolution of marine hard substrate communities: *Earth-Science Reviews*, v. 62, p. 1–103.
- TOBIN, K.J., WALKER, K.R., STEINHAUFF, D.M., AND MORA, C.I., 1996, Fibrous calcite from the Ordovician of Tennessee: preservation of marine oxygen isotopic composition and its implication: *Sedimentology*, v. 43, p. 235–251.
- TUCKER, M.E., 1974, Sedimentology of Palaeozoic pelagic limestones: the Devonian Griotte (southern France) and Cephalopodenkalk (Germany), in Hsu, K.J., and Jenkyns, H.C., eds., *Pelagic Sediments: on Land and under the Sea*, International Association of Sedimentologists, Special Publication 1, p. 71–92.
- VECSEI, A., 2003, Nutrient control of the global occurrence of isolated carbonate banks: *International Journal of Earth Sciences (Geologische Rundschau)*, v. 92, p. 476–481.
- WALLS, R.A., AND BURROWS, G., 1985, The role of cementation in the diagenetic history of Devonian reefs, western Canada, in Schneidermann, N., and Harris, P.M., eds., *Carbonate Cements*, SEPM, Special Publication 36, p. 185–220.
- WEBB, G.E., 1996, Was Phanerozoic reef history controlled by the distribution of non-enzymatically secreted reef carbonates (microbial carbonate and biologically induced cement)?: *Sedimentology*, v. 43, p. 947–971.
- WIEDENMAYER, F., 1963, Obere Trias bis mittlerer Lias zwischen Saltrio und Tremona (Lombardische Alpen)—die Wechselbeziehungen zwischen Stratigraphie, Sedimentologie und syngenetischer Tektonik: *Eclogae Geologicae Helveticae*, v. 56, p. 529–640.
- WILSON, P.A., AND DICKSON, J.A.D., 1996, Radial calcite: alteration product of and petrographic proxy for magnesian calcite marine cement: *Geology*, v. 24, p. 945–948.
- ZEEH, S., BECHSTÄDT, T., MCKENZIE, J., AND RICHTER, D.K., 1995, Diagenetic evolution of the Carnian Wetterstein platforms of the Eastern Alps: *Sedimentology*, v. 42, p. 199–222.